THE UNIVERSITY OF CHICAGO

DISTRIBUTIONAL STRESS-ENERGY IN GENERAL RELATIVITY AND ITS IMPLICATIONS FOR QUANTUM GRAVITY

A DISSERTATION SUBMITTED TO
THE FACULTY OF THE DIVISION OF THE PHYSICAL SCIENCES
IN CANDIDACY FOR THE DEGREE OF
DOCTOR OF PHILOSOPHY

DEPARTMENT OF PHYSICS

BY
KRISTIAN MACKEWICZ

CHICAGO, ILLINOIS
AUGUST 2024

I dedicate this doctoral thesis to my family and friends. An extra feeling of gratitude to my parents, Linda and Carl, who instilled in me the important values and qualities necessary to persevere facing any challenge. An additional appreciation for my many gym friends and colleagues, who all provided a fun and healthy escape from my endless work and helped keep me sane throughout this process.

“If we knew what it was we were doing, it would not be called research, would it?" -Albert Einstein

TABLE OF CONTENTS

LIST OF FIGURES

ACKNOWLEDGMENTS

First and foremost, I would like to acknowledge Dr. Craig Hogan for his unwavering support and for giving me the space to both fail and succeed and learn along the way.

I would also like to thank all of my committee members: Dr. Robert Wald, Dr. Daniel Holz, and Dr. Emil Martinec for their insightful feedback and for challenging me to adhere to a high standard of academic rigor. In particular, I am grateful to Dr. Robert Wald for his many helpful discussions on my research.

Finally, I am grateful for the many insightful discussions shared with the students of the Wald group over the years.

ABSTRACT

We review the current state of the art of techniques in general relativity involving null and/or distributional sources of stress-energy, with an emphasis on the study of gravitational shockwaves. We then propose a series of unsolved problems in which these techniques can be applied to uncover novel features of causal structure. In particular, we demonstrate methods in which the gravitational field due to quantum fluctuations can be modeled under the assumption that gravity is coherent over causal diamonds.

The first example studied is the decay of a particle with mass M into two counter-propagating null point particles. The resulting spherical shockwave is shown to produce displacement and velocity memory on a system of spherically arranged, synchronized clocks. We then consider quantum superpositions of decay axes and demonstrate that fluctuations of time shifts measured on the system of clocks should scale like $\langle \delta\tau^2 \rangle / \tau^2 \sim t_p/\tau$ in the limit of Planck mass particles.

The second problem studied is the gravitational effect of a "bubble model" representing the effective stress-energy of a pion. It is shown that such a model produces a mean secular outward acceleration of nearby test bodies that is consistent with the relative acceleration of bodies due to the cosmological constant.

NOTATION AND CONVENTIONS

Throughout this thesis, we will be using the metric signature $(-,+,+,+)$. Tensor indices are raised and lowered with the metric tensor g_{ab}, except in the linearized regime where the flat spacetime metric η_{ab} is used.

$\partial_a = {}_{,a} \equiv \frac{\partial}{\partial x^a}$	Coordinate Derivative Operator
δ_{ab}	Identity Matrix/Flat Space-Space Metric
$v^a v_a \equiv v^a v^b g_{ab} \equiv \sum_{a,b=0}^{3} v^a v^b g_{ab}$	Contraction, Eistein Summation Convention
$\gamma = (1 - v^2)^{-1/2}$	Lorentz Boost Factor
$\Box \equiv \nabla^a \nabla_a$	Wave Operator
$\mathbb{R}$	Set of Real Numbers
$\mathbb{R}^n$	Set of n-Tuples of Real Numbers
$\otimes$	Tensor Product of Vector Fields
$\frac{D}{D\tau} \equiv u^a \nabla_a$	Directional/Advective Derivative
$\int \delta(x - x_0) f(x) dx \equiv f(x_0)$	Dirac Delta Function

INTRODUCTION

Some of the very first studies of exact solutions to the Einstein field equations for gravitational plane waves date back to the work of Rosen [1937]. Originally, it was thought that such plane wave solutions were unphysical, but more recent work such as Bondi [1957] has demonstrated that plane wave solutions to the vacuum Einstein equations do exist. This family of solutions later came to be known as PP (parallel propagating plane-fronted) wave spacetimes [Ehlers and Kundt, 1962]. A more recent review on PP wave spacetimes can be found in Steele [1989]. It was then demonstrated by Aichelburg and Sexl [1971] that the speed of light limit of the boosted Schwarzschild solution produces an impulsive plane wave solution, otherwise known as a gravitational shockwave. This solution was the first attempt to characterize the gravitational effect of a null point particle. These shockwave solutions were then studied in further detail in Dray and 't Hooft [1985], Gemelli [1997]. More recently, shockwaves have been studied in the context of collisions [Barrabès and Hogan, 2011, Barrabès and Hogan, 2015], the memory effect at null infinity [Tolish and Wald, 2014, Tolish et al., 2019], and back reaction effects in black hole evaporation ['t Hooft, 2016b,a, 2018].

There have been other works characterizing solutions to the Einstein field equations for more general distributional stress-energy [Garfinkle, 1999, Geroch and Traschen, 1987]. As demonstrated in these works, there are many mathematical difficulties treating distributional sources in non-linear differential equations. In particular, products of distributions are not always mathematically well defined. Further, ambiguities arise even in the linearized theory for distributional sources since the notion of "small" is not well defined for distributional sources. Nevertheless, it was shown that unique solutions can exist for a certain class of distributional stress-energies.

Another important discovery in the realm of distributional stress-energy in general relativity was the formulation of what is now known as the Israel junction conditions. It was shown by Israel [1966], that one can join two spacetimes together in such a way that the

metric can be made continuous across the joining boundary, but there may be distributional curvature on the boundary. This result was extended even further to the case when the joining boundary is a null hypersurface [Barrabès and Israel, 1991, Barrabes, 1989, Poisson, 2002, Clarke and Dray, 1987]. When the curvature cannot be made continuous across these hypersurfaces, there must be an effective stress-energy that lives on the boundary. One can think of this stress-energy as sourcing a jump in the normal direction of the extrinsic curvature, similar to how a surface charge produces a jump in the normal component of the electric field (the gradient of the potential in the normal direction to the boundary) in classical electromagnetism.

We now outline the two novel problems in which these techniques will be applied to gain new insights. First, a linear analytical solution is derived for the gravitational shock wave produced by a particle of mass M that decays into a pair of point null particles. The resulting space-time is shown to be unperturbed and isotropic, except for a discontinuous perturbation on a spherical null shell. Formulae are derived for the perturbation as a function of polar angle, as measured by an observer at the origin observing clocks on a sphere at distance R. The effect of the shock is interpreted physically as an instantaneous displacement in time and velocity when the shock passes the clocks. The time displacement is shown to be anisotropic, dominated by a quadrupole harmonic aligned with the particle-decay axis, with a magnitude $\delta\tau \sim GM/c^3$, independent of R. The velocity displacement is isotropic. The solution is used to derive the gravitational effect of a quantum state with a superposition of a large number of randomly oriented, statistically isotropic particle decays. This approach is shown to provide a well-controlled approximation to estimate the magnitude of gravitational fluctuations in systems composed of null point particles up to the Planck energy in a causal diamond of duration $\tau = 2R/c$, as well as quantum-gravitational fluctuations of black holes and cosmological horizons. Coherent large-angle quantum distortions of macroscopic geometry from fluctuations up to the Planck scale are shown to grow linearly with the duration, with

a variance $\langle \delta\tau^2 \rangle \sim \tau t_P$ much larger than that produced in models without causal quantum coherence.

Finally, we analyze the classical linear gravitational effect of idealized pion-like dynamical systems, consisting of light quarks connected by attractive gluonic material with a stress-energy $p = -\rho c^2$ in one or more dimensions. In one orbit of a system of total mass M, quarks of mass $m << M$ expand apart initially with $v/c \sim 1$, slow due to the gluonic attraction, reach a maximum size $R_0 \sim \hbar/Mc$, then recollapse. We solve the linearized Einstein equations and derive the effect on freely falling bodies for two systems: a gluonic bubble model where uniform gluonic stress-energy fills a spherical volume bounded by a 2D surface comprising the quarks' rest mass, and a gluonic string model where a thin string connects two pointlike quarks. The bubble model is shown to produce a secular mean outward residual velocity of test particles that lie within its orbit. It is shown that the mean gravitational repulsion of bubble-like virtual-pion vacuum fluctuations agrees with the measured value of the cosmological constant, for a bubble with a radius equal to about twice the pion de Broglie length. These results support the conjecture that coherent gravity of standard QCD vacuum fluctuations is the main source of cosmic acceleration.

0.1 Mathematical preliminaries

Before we begin, we review some mathematical preliminaries of the theory of general relativity that will be used extensively throughout the work. Much of the notation in this manuscript will be borrowed from Wald [1984], though there will occasionally be some deviations, particularly in the notation for the metric perturbation.

We consider spacetime manifolds, $\mathcal{M}$, with associated spacetime metric g_{ab}. From Wald [1984], an n dimensional, C^∞, real manifold is a set of points p, along with a collection of subsets $\{O_\alpha\}$ such that: 1) the $\{O_\alpha\}$ cover $\mathcal{M}$, 2) for each α, there is a bijective map $\psi_\alpha : O_\alpha \to U_\alpha$, where U_α is an open subset of $\mathbb{R}^n$, and 3) the transfer functions $\psi_\alpha \circ \psi_\beta^{-1}$:

$\mathbb{R}^n \to \mathbb{R}^n$ must be C^∞ in their domain of definition. These conditions can be relaxed to suitably define a distributional solution for the spacetime metric.

The points in the manifold are commonly referred to as spacetime events. The maps ψ_α are referred to as charts, or coordinate systems. The infinitesimal distance function between events, known as the spacetime interval, is defined by

$$ds^2 = g_{ab} dx^a dx^b \tag{1}$$

where the Einstein summation convention is used. The "distance" between points connected by a curve parameterized by λ is then

$$s = \int_{\lambda_1}^{\lambda_2} \sqrt{\pm g_{ab} \frac{dx^a}{d\lambda} \frac{dx^b}{d\lambda}} d\lambda \tag{2}$$

The plus sign is to be taken for events that are spacelike separated (the distance defines proper length), while the minus sign should be taken for events that are timelike separated (the distance defines proper time). Two events are said to be null separated if the spacetime "distance" is zero.

The relation between matter and the geometrical structure of spacetime is defined via the Einstein field equations

$$G_{ab} \equiv R_{ab} - \frac{1}{2} R g_{ab} = 8\pi T_{ab} \tag{3}$$

where T_{ab} is the stress-energy tensor, which is a conserved quantity satisfying

$$\nabla^a T_{ab} = 0 \tag{4}$$

where ∇_a is the covariant derivative operator, which is a map from tensors of rank (k, l) to tensors of rank $(k, l+1)$ satisfying three properties: 1) linearity, 2) the Leibniz rule,

and 3) commutativity with contraction of indices. A tensor of rank (k, l) at a point p is a multi-linear map between k dual vectors and l vectors to real numbers.

$$T^{a_1...a_k}_{b_1...b_l} : \underbrace{V \otimes ... \otimes V}_{l} \underbrace{\otimes V^* \otimes ... \otimes V^*}_{k} \to \mathbb{R} \tag{5}$$

A tensor can be written as a linear combination of tensor products of vector basis elements e^a_μ and dual vector basis elements e^ν_b, where $e^a_\mu(e^\mu_b) \equiv \delta^a_b$.

$$T^{a_1...a_k}_{b_1...b_l} = \sum C^{\mu_1...\mu_k}_{\nu_1...\nu_l} e^{\nu_1}_{b_1} \otimes ... \otimes e^{\nu_k}_{b_l} \otimes e^{a_1}_{\mu_1} \otimes ... \otimes e^{a_k}_{\mu_k} \tag{6}$$

Typically, the stress-energy tensor is assumed to be smooth (C^∞) and of compact support. However, in this manuscript we will primarily be considering stress-energy tensors whose components are distributional, i.e. they are not smooth functions and their meaning is to be taken relative to integration over an appropriate class of test functions (e.g. the Dirac delta function).

Geodesics of the spacetime with tangent vector u^a satisfy the geodesic equation

$$u^b \nabla_b u^a = \frac{d^2 x^a}{d\tau^2} + \Gamma^a_{bc} \frac{dx^b}{d\tau} \frac{dx^c}{d\tau} = 0 \tag{7}$$

where the Christoffel symbols Γ^a_{bc} are defined by

$$\Gamma^a_{bc} = \frac{1}{2} g^{ad} (\partial_b g_{dc} + \partial_c g_{db} - \partial_d g_{bc}) \tag{8}$$

Two initially parallel geodesics with tangent vector u^a and displacement vector D^a will evolve in time according to the geodesic deviation equation

$$u^c \nabla_c (u^b \nabla_b D^a) = -R_{bdc}{}^a u^b u^c D^d \tag{9}$$

where $R_{abc}{}^{d}$ is the Riemann curvature tensor associated with the spacetime.

$$R_{abc}{}^{d} = \partial_b \Gamma^d_{ac} - \partial_a \Gamma^d_{bc} + \Gamma^d_{ea}\Gamma^e_{bc} - \Gamma^d_{eb}\Gamma^e_{ac} \tag{10}$$

For most of this thesis, we will be primarily concerned with perturbations off a flat background spacetime. We can then define a metric perturbation h_{ab} such that

$$g_{ab} = \eta_{ab} + h_{ab} \tag{11}$$

where h_{ab} is small in some suitable sense. For notational convenience, we can define the trace-reversed metric perturbation

$$\bar{h}_{ab} = h_{ab} - \frac{1}{2} h \eta_{ab} \tag{12}$$

To linear order in h_{ab}, the Einstein field equations reduce to a wave equation sourced by the stress-energy tensor. As is well known in the theory, two metrics are physically equivalent if they can be related via a gauge transformation of the form

$$g_{ab} \to g_{ab} + \nabla_a \xi_b + \nabla_b \xi_a \tag{13}$$

While working with the linearized field equations, we can define the Lorenz gauge such that $\nabla^a \bar{h}_{ab} = 0$. In this gauge, the linearized Einstein field equations become

$$\Box \bar{h}_{ab} = -16\pi T_{ab} \tag{14}$$

With suitable boundary conditions, we can invert the wave operator and determine an inte-

gral solution for the metric perturbation.

$$\bar{h}_{ab} = 4 \int \frac{T_{ab}(x', t_{\rm ret}(x'))}{|x' - x|} d^3x' \tag{15}$$

The linearized Christoffel symbols are

$$\Gamma^a_{bc} = \frac{1}{2}\eta^{ad}(\partial_b h_{dc} + \partial_c h_{db} - \partial_d h_{bc}) \tag{16}$$

The linearized Riemann tensor is

$$R_{abcd} = 2\nabla_{[a}\nabla_{[d}h_{c]b]} \tag{17}$$

Throughout this manuscript, factors of c, G and later $\hbar$ will frequently be omitted during calculations, but are retained for key physical formulae.

CHAPTER 1

GRAVITY OF TWO PHOTON DECAY

1.1 Introduction

One of the simplest exact solutions of Einstein's equations is the planar gravitational shock wave produced by a point particle on a null trajectory [Aichelburg and Sexl, 1971, Dray and 't Hooft, 1985]. This idealized system has been applied to study the "memory effect" at null infinity [Tolish and Wald, 2014, Satishchandran and Wald, 2019], and extrapolated to quantum systems, including the back-reaction of particle emission on the horizon of a black hole ['t Hooft, 2016b,a, 2018].

Here, we analyze the solution for the spherical gravitational shock wave produced by a pair of oppositely-propagating point null particles originating from a single point mass at rest in a nearly-flat space-time background. We evaluate the effect of the shock on a sphere at a finite distance R, and the observable distortion of space-time geometry on that sphere as function of direction and time, as observed at the origin.

In this system, the memory effect takes the form of an anisotropic distortion of time.The distortions can be characterized by a local measurement with a simple operational definition. Before the particle decays, a sphere of clocks is synchronized by an outgoing spherical pulse from the origin. After the particle decays, the gravity of the shock distorts the measured time on clocks in all directions, compared synchronously on the world line of an inertial observer at the origin.

We choose to study this system in particular because it is well suited to study the relationship of space-time with causally-coherent quantum states of gravitating mass-energy. Unlike the planar shock solution, all of the elements of the system are contained in a compact causal diamond of space-time. In this set-up, an entire quantum system, including preparation and measurement of a state and a measurement apparatus, can be incorporated

into a gravitational solution: both the preparation of the state and the measurement of the gravitational perturbation response are localized on a single world line, in an interval of finite duration. In other words, the solution describes a locally-measurable timelike response to a nonlocal spacelike gravitational effect.

This solution is applied below to estimate the effect of causally-coherent quantum nonlocality on gravitational fluctuations. Our estimate of the gravitational fluctuations is based on the correspondence principle, the hypothesis that the quantum state of a whole system can be expressed as a superposition of consistent classical histories of matter and space-time. The main conclusions are thus insensitive to the unknown detailed structure of nonlocal quantum states in curved space-time [Pikovski et al., 2017, Banks, 2020], as long as they are causally coherent.

Previous model systems do not have the causal structure required for this exercise. The initial conditions for the source in the classical planar shock solution [Aichelburg and Sexl, 1971, Dray and 't Hooft, 1985], a null point particle, cannot be set up causally in a quantum system: a definite direction for the particle momentum requires that its quantum state be delocalized everywhere on planes normal to the direction of travel. Similarly, the standard approach to nonlocality adopted in effective field theory, widely used to study gravitational fluctuations in cosmic inflation [Weinberg, 2008b, Baumann, 2011], quantizes coherent, infinite plane wave modes, not superpositions of directional particle states confined to causal diamonds.

The angular structure of the spherical null gravitational shock displays a large-angle coherence that is not captured by such models based on nonlocal planar symmetry. The spherical null shock relates a causal, nonlocal effect of gravity to localized pointlike events. The anisotropic, coherent angular gravitational effects in relation to a point are confined to a null surface, and also extend to macroscopic separation. The solution is consistent with general relativity and quantum mechanics for particles up to the Planck mass, so it is

a suitable approximation to estimate large-angle correlations of causally-coherent quantum gravity and its fluctuations in macroscopic systems.

The classical single-particle decay solution is used here to estimate coherent nonlocalized quantum-gravitational effects of quantum superpositions of matter states. We apply the classical solution to two quantum systems, an S-wave decay with an isotropic directional wave function, and the sequential isotropic decay of many such particles originating on the same world line. These solutions allow us to derive the large-angle correlations of the quantum-gravitational response to a many-particle state.

Assuming that relativity and quantum mechanics are valid and obey the correspondence principle, a superposition of these solutions approximately describes the coherent state of a quantum geometry, up to the point where the total mass of particles approaches that of a black hole for the duration defined by the measurement. The extrapolation to many particles provides a controlled estimate of macroscopic quantum fluctuations of causally-coherent, weak-field gravity for systems of any size. The estimate here shows a variance of large-angle, macroscopic distortions on the surface of a causal diamond that grows linearly with its duration, which agrees with recent estimates based on conformal descriptions of near-horizon vacuum states [Banks and Zurek, 2021], but is much larger than estimates from field theory [Weinberg, 2008b, Baumann, 2011] that do not include the same causal coherence. This difference is in principle measurable, and might have observable consequences.

1.2 Setup and General Properties of the Solution

Consider the system shown in fig. 1.1. A particle of mass M at the origin is surrounded by a set of clocks distributed on a sphere of radius R. The clocks are synchronized by a pulse from the origin prior to t_0. The clocks are on freely falling timelike geodesics.

At a time t_0, the particle decays into a pair of equal-momentum null point particles that propagate in opposite directions along the z axis. The particles create an outgoing spher-

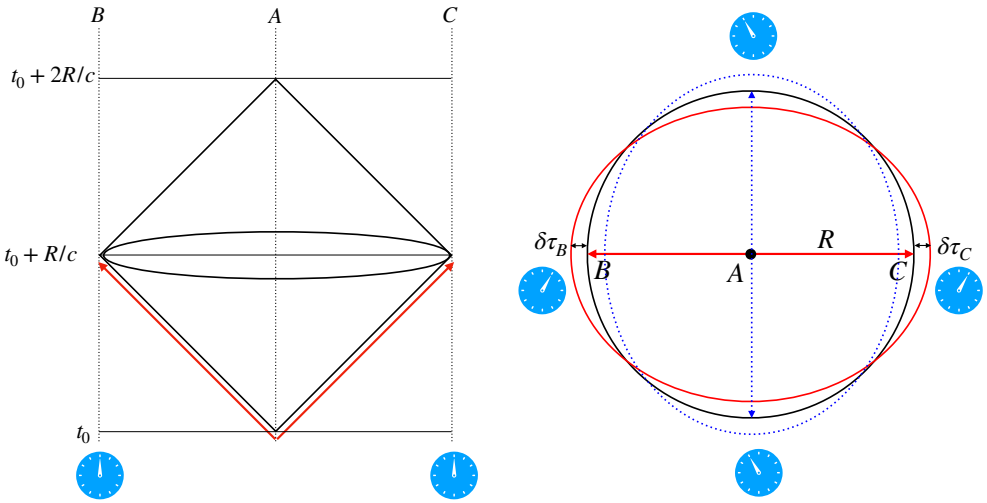

Figure 1.1: Gravitational effect of a particle pair on observed time perturbations. At left, a point mass on world line A decays at t_0 into oppositely directed null particles. A time R/c later, the gravitational shock wave of the particles creates a coherent perturbation on the spherical boundary of a causal diamond of radius R, as shown at the right. Clocks on the surface are synchronized by an outwards pulse from A just before t_0, and observed by A by return light from the surface of the causal diamond after $t_0 + 2R/c$. The shock creates coherent time displacements with an even-parity directional variation of amplitude $\delta\tau \sim GM/c^3$ aligned with the particle trajectory, as shown by comparing on-axis clocks at B and C with those in equatorial directions.

ical gravitational shock wave that creates a direction-dependent discontinuity in timelike geodesics as it passes. Outside the shock wave, the solution is a Schwarzschild space-time of mass M; inside, the solution is a flat space-time.

When the shock passes through R, the sphere of clocks is perturbed. The shock creates an instantaneous displacement of position and velocity that depends on the angle from the particle axis. The bulk of the total displacement measured as a difference between clocks occurs on large angular scales, that is, in low spherical harmonics, dominated by a quadrupole or tidal term. The physical effect of the shock wave can be visualized as a coherent, anisotropic, discontinuous displacement of time on the order of $\delta\tau \sim GM/c^3$, together with an isotropic redshift discontinuity $\delta\tau/\tau \sim GM/Rc^2$ that represents the disappearance of gravitational redshift in the post-shock solution.

1.3 Spacetime Geometry

1.3.1 Metric Perturbation

Consider a particle with mass M sitting at rest at position $z = t_0$ of global inertial coordinates (t, x, y, z). At time $t = t_0$, the particle decays into two massless particles with energy $E = M/2$ that propagate in opposite directions along the z axis. We assume that M is small so that we may use the weak field approximation to determine the spacetime geometry. We will look for the solution to the linearized Einstein equations in the Lorenz gauge $\nabla^a \bar{h}_{ab} = 0$, i.e. solutions to eq. (14). The spacetime diagram for this event is given by fig. 1.2.

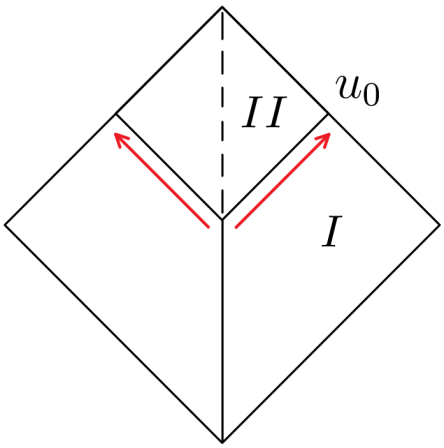

Figure 1.2: Penrose diagram of decay process. A stationary massive particle sits at the origin (solid world line) and decays at retarded time u_0, producing two oppositely propagating null particles. An observer remains at rest at the origin (dashed word line). The null hypersurface created by the spherically propagating shock wave separates the two spacetime regions I (Schwarzschild) and II (Minkowski).

The stress-energy tensor for the system described is

$$T^{ab} = M\delta(x)\delta(y)\left[\delta(z)\theta(-t)t^a t^b + \frac{1}{2}(\delta(z+t)l^a l^b + \delta(z-t)k^a k^b)\theta(t)\right] \tag{1.1}$$

where $k^a = t^a + z^a, l^a = t^a - z^a$, and $\theta(t)$ is a Heaviside step function (for simplicity we have set $t_0 = 0$). For $t < 0$, this is the usual stress-energy for a point particle (at rest) given by

$T^{ab} = \gamma m v^a v^b \delta^{(3)}(\mathbf{x} - \mathbf{x}(\tau))$. For $t > 0$, this is the generalization of the previous formula to the massless limit, taking $\gamma m \to E$.

We can solve this wave equation term by term by letting $\bar{h}^I_{ab} = f_I(x^c) t_a t_b$, $\bar{h}^{II}_{ab} = f_{II}(x^c) l_a l_b$, $\bar{h}^{III}_{ab} = f_{III}(x^c) k_a k_b$. We then have three sourced scalar wave equations with sources S_i which contain the information of the stress-energy tensor.

$$\Box f_i = -4\pi S_i \tag{1.2}$$

The retarded Green's function for the $\Box$ operator is

$$G_R(t, \vec{x};, t', \vec{x}\,') = \frac{1}{2\pi} \delta(-(t - t')^2 + |\vec{x} - \vec{x}\,'|^2) \theta(t - t') \tag{1.3}$$

The solutions to eq. (1.2) are given by

$$f_i(x) = 4\pi \int d^4x' G(t, \vec{x}; t', \vec{x}\,') S_i(t', \vec{x}\,') \tag{1.4}$$

The complete metric perturbation is then given by Tolish and Wald [2014]

$$h_{ab} = \frac{2M}{r}(\eta_{ab} + 2t_a t_b)\theta(-U) + \frac{2M}{t+z} l_a l_b \theta(U) + \frac{2M}{t-z} k_a k_b \theta(U) \tag{1.5}$$

where $U = t - r$ and $r = (x^2 + y^2 + z^2)^{1/2}$. The step function behavior indicates that the spacetime will be that of a spherically propagating shock wave. Although at first glance it appears as though the spacetime inside the shock wave ($U > 0$) is not flat, one can make an appropriate coordinate transformation to show that the metric is indeed that of a flat spacetime. We have in null coordinates $u = t - z, v = t + z$

$$ds^2(U > 0) = -dudv + \frac{2M}{u} du^2 + \frac{2M}{v} dv^2 + dx^2 + dy^2 \tag{1.6}$$

We now define new null coordinates as in Dray and 't Hooft [1985]

$$d\tilde{v} = dv - \frac{2M}{u}du \quad d\tilde{u} = du - \frac{2M}{v}dv \tag{1.7}$$

Since we are in the linearized regime, we drop terms $\mathcal{O}(M^2)$. The spacetime metric in the new null coordinates becomes

$$ds^2(U > 0) = -d\tilde{u}d\tilde{v} + dx^2 + dy^2 \tag{1.8}$$

Aside from the discontinuity at $u = 0, v = 0$ in the new null coordinates $\tilde{u}, \tilde{v}$, we see that the spacetime is flat to the causal future of the decay event (henceforth referred to as "inside" the shock wave). In the next section we will again demonstrate this by showing that the Riemann tensor vanishes inside the shock wave.

We briefly mention here that eq. (1.5) agrees with the metric perturbation derived in Rätzel et al. [2017] after carefully taking the limit $L \to 0, \epsilon \to M/2$, where L corresponds to the width of the laser pulse considered in their work, and ϵ is the energy of each pulse. Note that while the metric perturbation can me made continuous in their system, the limit $L \to 0$ makes the metric perturbation have a discontinuous jump at $U = t - r = 0$.

1.3.2 Geodesic Deviation

We now determine the relative motion of test bodies in this spacetime (note that in all calculations we raise and lower indices with η_{ab}). Consider a congruence of timelike geodesics that are initially "at rest", with spatial deviation vector D^a. Define the tangent to the world line of a test clock by u^a. Initially, we have $u^a_0 = t^a = (1, 0, 0, 0)$. The deviation evolves according to the geodesic deviation equation eq. (9).

Since the clocks will be allowed to free-fall after the system is set up, the tangents to the world lines will pick up $\mathcal{O}(M/r)$ corrections between the time of release and the time

of the shock wave passing by. However, we can ignore this correction to the velocity when computing displacement/velocity kicks so long as the free-fall time is not too long since we only care about the leading order effect and the Riemann tensor is at least $\mathcal{O}(M/r)$.

There will be three types of terms in the Riemann tensor components. One type will be proportional to a step function, which gives the usual gravitational tidal force. The second type will be proportional to a δ function, which results in a relative velocity kick. The third type will be proportional to the derivative of a δ function, which results in a relative displacement kick: this is the memory effect. We can write the displacement vector as

$$D^a = D^a_{(0)} + D^a_{(1)} + D^a_{(2)} + D^a_{(3)} \tag{1.9}$$

where the (n) refers to the $1/r^n$ piece. We consider changes to D^a to linear order in M only. In what follows, we use the following convention for coordinate vectors: $\nabla^a z = z^a, \nabla^a t = -t^a \Rightarrow \nabla^a u = -k^a, \nabla^a v = -l^a$.

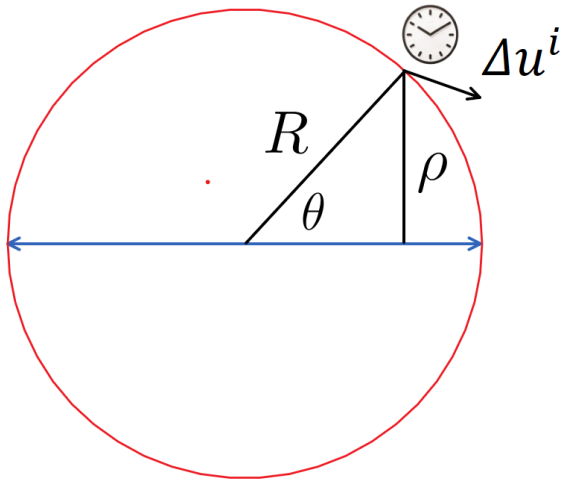

Figure 1.3: Two oppositely-propagating massless particles (blue) creating a spherically symmetric gravitational shock wave (red). The clocks sitting at radius R experience an instantaneous displacement (not shown) and velocity kick Δu^i as a function of angle θ.

The curvature components proportional to a derivative of a δ function come from both

derivatives acting on the step function.

$$\nabla_a H(U) = \delta(U)\nabla_a U \tag{1.10}$$

$$\nabla_d \nabla_a H(U) = \delta'(U)\nabla_d U \nabla_a U + \delta(U)\nabla_d \nabla_a U \tag{1.11}$$

Note that since we will ultimately be antisymmeterizing on pairs of indices, we can treat the covariant derivatives as coordinate derivatives in computing the Riemann tensor components. We focus attention on the first term for now. $\nabla_a U = -(t_a + r_a) = -K_a$. Note that at $t = r$, we have $u = r - z = r(1 - \cos\theta), v = r + z = r(1 + \cos\theta)$. Plugging into eq. (10) gives

$$\begin{aligned} R^{\delta'}_{abcd} = &-\frac{4M}{r}(K_{[a}\eta_{b][c}K_{d]} + 2K_{[a}t_{b]}t_{[c}K_{d]})\delta'(t-r) \\ &+ \frac{4M}{r}\left(\frac{1}{1-\cos\theta}K_{[a}k_{b]}k_{[c}K_{d]} + \frac{1}{1+\cos\theta}K_{[a}l_{b]}l_{[c}K_{d]}\right)\delta'(t-r) \end{aligned} \tag{1.12}$$

If we consider the components of D^a in a parallelly propagated orthonormal frame, the left hand side of eq. (9) reads d^2D^a/dt^2. Integrating the geodesic deviation equation twice gives

$$(\Delta D_{(1)})_a = \frac{M}{r}(\theta_a\theta_b - \phi_a\phi_b)D^b_{(0)} \tag{1.13}$$

where θ_a, ϕ_a are the unit tangent vectors on the sphere. Thus, there is an instantaneous relative displacement kick between two nearby stationary test bodies.

As shown in the appendix, we can decompose this tensor into a tensor harmonic mode sum. Specifically, the displacement kick can be decomposed into a sum over transverse "electric" tensor harmonics. The coefficients of the mode sum are given by eq. (A.26):

$$\Delta D = -\frac{M}{r}(\hat\theta\hat\theta - \hat\phi\hat\phi)\cdot D_{(0)} \sum_{l=2,\text{even}}^{\infty} \frac{2l+1}{l(l-1)(l+1)(l+2)}\left(2\cot\theta\frac{d}{d\theta} + l(l+1)\right)P_l(\cos\theta) \tag{1.14}$$

where $\hat{\phi}, \hat{\theta}$ are angular unit vectors on the sphere. The quadrupolar mode ($l = 2$) gives

$$\Delta D_{l=2} = \frac{5M}{8r}\sin^2\theta(\hat{\theta}\hat{\theta} - \hat{\phi}\hat{\phi})\cdot D_{(0)} \tag{1.15}$$

We note here that one could attempt to "glue" the two spacetime regions (Minkowski and Schwarzschild) together using the formalism developed by Barrabès and Israel [1991]. The results of their work indicate that the Riemann tensor is at most δ function singular on the null boundary when the induced metric on the null hypersurface joining the two spacetimes can be made continuous. However, as shown in Satishchandran and Wald [2019], there must be a change in the leading order metric (which is associated with memory) for the type of stress-energy considered here. Therefore, the metric cannot be made continuous here and there will be a δ' type singular behavior on the null hypersurface.

The curvature components proportional to a δ function come from the second term in eq. (1.11) and the cross term when acting two derivatives on h^I_{ab} in eq. (1.5). Again, derivatives acting on $1/u, 1/v$ will not contribute since they are proportional to k^a, l^a respectively. In addition to the terms mentioned above, there will be a term proportional to $\delta(t-r)$ that comes from integration by parts of the terms proportional to $\delta'(t-r)$ when integrating the geodesic deviation equation:

$$\begin{aligned} R^{\delta}_{abcd} = &\frac{4M}{r^2}(\theta_{[a}(\eta_{b][c} + 2t_{b]}t_{[c})\theta_{d]} + \phi_{[a}(\eta_{b][c} + 2t_{b]}t_{[c})\phi_{d]}) \\ &- \frac{4M}{r^2}(K_{[a}(\eta_{b][c} + 2t_{b]}t_{[c})r_{d]} + r_{[a}(\eta_{b][c} + 2t_{b]}t_{[c})K_{d]}) \\ &- \frac{4M}{r^2(1-\cos\theta)}(\theta_{[a}k_{b]}k_{[c}\theta_{d]} + \phi_{[a}k_{b]}k_{[c}\phi_{d]}) \\ &- \frac{4M}{r^2(1+\cos\theta)}(\theta_{[a}l_{b]}l_{[c}\theta_{d]} + \phi_{[a}l_{b]}l_{[c}\phi_{d]}) \\ &+ \frac{4M}{r^2(1-\cos\theta)^2}K_{[a}k_{b]}k_{[c}K_{d]} + \frac{4M}{r^2(1+\cos\theta)^2}K_{[a}l_{b]}l_{[c}K_{d]} \end{aligned} \tag{1.16}$$

Again, keeping only the leading order behavior in $1/r$ and integrating the geodesic deviation

equation once then gives

$$\Delta v_a^{(2)} = \frac{M}{r^2}\left[(\theta_a\theta_b - \phi_a\phi_b)\frac{1+\cos^2\theta}{1-\cos^2\theta} + \frac{2\sin\theta\cos\theta}{1-\cos^2\theta}(r_a\theta_b + r_b\theta_a)\right] D^b_{(0)}. \tag{1.17}$$

Thus, there is an instantaneous relative velocity kick between two nearby stationary test bodies as measured in a parallelly propagated frame.

The curvature components proportional to a step function come from both derivatives hitting the pre-factors in eq. (1.5). Only the first piece of h_{ab} will contribute since $\nabla^a u = -k^a$, etc., and the antisymmetrization will kill these terms. The Riemann tensor associated with tidal forces is

$$R^{\text{tid}}_{abcd} = \frac{4M}{r^3}(\eta_{[a[d} + 2t_{[a}t_{[d})(\delta_{b]c]} - 3r_{b]}r_{c]})\theta(-(t-r)) \tag{1.18}$$

Finally, eq. (9) gives

$$\frac{d^2 D^{(3)}_a}{dt^2} = \frac{M}{r^3}(2r_a r_b - \theta_a\theta_b - \phi_a\phi_b)D^b_{(0)}\theta(-(t-r)) \tag{1.19}$$

This is the usual form of tidal forces in Newtonian gravity. Note that this term "turns off" after the shock has passed a given test body.

1.4 Time Displacement

Consider a system of synchronized clocks distributed on a sphere of radius r. After the passage of the gravitational shock wave, the clocks will no longer be synchronized due to the relative displacement kick. The desynchronization of clocks on the sphere can be determined via supertranslations at future null infinity, or $\mathcal{I}^+$ [Strominger and Zhiboedov, 2014]. These are asymptotic symmetries (part of the BMS group) of asymptotically flat spacetimes [Bondi

et al., 1962, Sachs, 1962]. The generator of these symmetries is given by

$$\psi^a = T(x^A)\left(\frac{\partial}{\partial u}\right)^a - T(x^A)\left(\frac{\partial}{\partial r}\right)^a - \frac{1}{r}\mathcal{D}^C T(x^A)\left(\frac{\partial}{\partial x^C}\right)^a + ... \tag{1.20}$$

which creates an infinitesimal shift in the retarded time

$$u \to u - T(\theta, \phi) \tag{1.21}$$

Here x^A are the position coordinates on the 2-sphere. In 4 spacetime dimensions, it has been shown that (null) memory is purely of scalar type, and can be written in terms of these supertranslations [Satishchandran and Wald, 2019]. The relation is given by

$$\Delta_{AB} = \frac{1}{r}\left(\mathcal{D}_A\mathcal{D}_B - \frac{1}{2}q_{AB}\mathcal{D}^2\right)T(\theta, \phi) \tag{1.22}$$

where $\mathcal{D}_A$ is the covariant angular derivative operator on the sphere [Hollands et al., 2016]. From eq. (18) we have

$$\Delta_{\theta\theta} = \frac{2M}{r}\sum_{l=2,\text{even}}^{\infty}\frac{2l+1}{l(l-1)(l+1)(l+2)}\left(\frac{d^2}{d\theta^2} + \frac{1}{2}l(l+1)\right)P_l(\cos\theta) \tag{1.23}$$

From this one can easily read off the $l > 1$ contributions to $T(\theta, \phi)$:

$$T(\theta, \phi) = T_{0,1} + 2M\sum_{l=2,\text{even}}^{\infty}\frac{2l+1}{l(l-1)(l+1)(l+2)}P_l(\cos\theta) \tag{1.24}$$

The $l = 0, 1$ contributions are due to standard temporal and radial spatial translations. By setting up our system of clocks on the sphere to be initially synchronized, these two terms vanish.

Equation (1.24) is the main result of this paper, the angular pattern of time displacement recorded on the surface of the causal diamond. Since the weighting falls off as $\sim 1/l^3$, the

$l = 2$ mode will be the dominant contribution. It has an angular dependence

$$T_2(\theta) = \frac{5M}{24}(3\cos^2\theta - 1). \tag{1.25}$$

1.5 Velocity Kick

Previously, we considered the relative velocity induced between nearby observers in a parallelly propagated frame. However, we would also like to know the (global) radial velocity (away form the origin) of each clock on the sphere, as this will produce a longitudinal Doppler shift as measured by the observer at the origin. We can determine the induced velocity $u^a = dx^a/dt$ of each clock by solving the geodesic equation.

$$\frac{du^a}{dt} + \Gamma^a_{bc} u^b u^c = 0 \tag{1.26}$$

where we have chosen to parameterize the worldlines by the coordinate time t. The tangent vector to the worldline of the clocks is initially given by that of a stationary observer, i.e. $u^a_0 = t^a$. Since the leading order corrections to u^a are $\mathcal{O}(M/r)$ and the linearized Christoffel symbols are also $\mathcal{O}(M/r)$, we can use u^a_0 in eq. (1.26). Therefore in our linearized regime we have

$$\frac{du^i}{dt} \approx -\Gamma^i_{tt} \tag{1.27}$$

where

$$\Gamma^i_{tt} = \frac{1}{2}(2\partial_t h_{it} - \partial_i h_{tt}) \tag{1.28}$$

We want to determine the instantaneous (globally measured) velocity kick, which comes from the Christoffel symbols proportional to delta functions. In Cartesian coordinates, we have

$$u^\mu = u^\mu_0 + \frac{M}{x^2+y^2}\left(\frac{r^2+z^2}{r^2}, -x\frac{r^2+z^2}{r^2}, -y\frac{r^2+z^2}{r^2}, z\frac{3r^2-z^2}{r^2}\right) \tag{1.29}$$

At this point we must discuss a subtle point about what the observer at the origin is measuring. As mentioned in section $IIIA$, the original coordinate chart (t, x, y, z) is not well suited to describe the flat spacetime that the observer at the origin is making measurements in. We want to know how fast a given clock is moving away from the origin as measured in time $\tilde{t}$. We need to make the appropriate coordinate transformation to the coordinates $(\tilde{t}, \tilde{x}, \tilde{y}, \tilde{z})$ and re-parameterize the worldline of the clocks.

$$\tilde{u}^a = \frac{dt}{d\tilde{t}} \frac{\partial \tilde{x}^a}{\partial x^b} u^b \tag{1.30}$$

Using eq. (1.7) we find that

$$\frac{\partial \tilde{x}^a}{\partial x^b} = \delta^a_b + \left(\frac{M}{u} + \frac{M}{v}\right)(z^a z_b - t^a t_b) + \left(\frac{M}{v} - \frac{M}{u}\right)(t^a z_b - z^a t_b) \tag{1.31}$$

$$\frac{d\tilde{t}}{dt} = u^a \nabla_a \tilde{t} = u^a \left(t_a \left(-1 + \frac{M}{u} + \frac{M}{v}\right) + z_a \left(\frac{M}{u} - \frac{M}{v}\right)\right) \tag{1.32}$$

In what follows, we expand everything out to $\mathcal{O}(M/r)$. In the new coordinates $(\tilde{t}, \tilde{x}, \tilde{y}, \tilde{z})$ we have

$$\tilde{u}^\mu = \left(1, -\frac{M}{r}\frac{1+\cos^2\theta}{1-\cos^2\theta}\sin\theta\cos\phi, -\frac{M}{r}\frac{1+\cos^2\theta}{1-\cos^2\theta}\sin\theta\sin\phi, \frac{M}{r}\cos\theta\right) \tag{1.33}$$

We note here that although we should have transformed (r, θ) into $(\tilde{r}, \tilde{\theta})$, the difference between these coordinates is $\mathcal{O}(M/r)$, so it is sufficient to use the original spherical polar coordinates to leading order (this is explained in more detail in the next section). As can be seen by eq. (1.33), there is an inward relative velocity transverse to the ϕ direction, with an outward velocity in the z direction. This distorts the sphere into an ellipsoidal shape. If one does a Taylor expansion about a particular point, they will recover the relative velocity kick between nearby observers derived in eq. (1.17).

Projecting the velocity kick into the radial and transverse directions, we get

$$\Delta u^r = -\frac{M}{r} \tag{1.34}$$

$$\Delta u^\theta = -\frac{2M}{r}\cot\theta \tag{1.35}$$

We find that the radial velocity kick is isotropic, while the transverse velocity kick is not isotropic and is badly divergent near the polar axes, which we discuss how to handle in the next section. This isotropic radial velocity kick can be decomposed into two parts, as demonstrated in Rätzel et al. [2017]: an outward impulse purely due to the loss of mass in the spacetime, and an inward impulse due to the propagating photon, whose gravity always points inwards and transverse to the z axis (i.e. in the $-\hat{\rho}$ direction). The net radial impulse is toward the origin, and since it is independent of polar angle, only the angular velocity kick "knows" about the location of the counter-propagating null particles - one can show that the relative kick in this direction given by the 2nd term in eq. (1.17) agrees with the result of Aichelburg and Sexl [1971] in the appropriate limit. Although the angular component is divergent at the poles, one can expand for small $\cos\theta$ (i.e. near the equator) to get an approximate solution. We comment here that the full solution to the non-linear Einstein equations (with smoothed source) should be regular at the poles and should match on to this expansion around the equator in the weak field limit.

The effect of the radial velocity kick is to produce a Doppler shift in the clocks relative to the central observer. All the clocks appear to run faster after the shock has passed; this can be interpreted as an inward velocity kick from the shock, which is indistinguishable from the disappearance of the isotropic gravitational redshift relative to the central observer that was present in the pre-shock system. The longitudinal Doppler shift is first order in the (radial) velocity, but the profile is spherically symmetric and thus the observer gains no information about which way the two particles went. If one considers many such decays

originating from the same point, there will be no fluctuations in this measurement. The transverse Doppler shift at leading order is second order in the (angular) velocity kick, so this will be a sub-leading effect (recall that $M/r << 1$ to satisfy the linearized regime).

We conclude that the anisotropic effects at leading order in M/r are due to the time shift induced by the relative displacement kicks of the clocks, which give rise to measurable angular fluctuations.

1.6 Limits of Validity

This solution is not exact. The linear approximation to gravity breaks down at large M, and because of quantum uncertainty, the point-particle approximation breaks down at small M. (We will continue to assume that the clocks are represented classically, as point-like tracers of local proper time; this does not affect our conclusions in the regime of interest.)

For a single particle decay, the linear approximation breaks down close to the axis [1]. It leads to unphysical effects if the impact parameter is less than the Schwarzschild radius for mass M: the scattering angle becomes large, and the orbits of clocks carry them across the singularity on the axis. Putting back the units, from eq. (1.5) we see that the linear approximation is valid only for

$$\frac{2GM}{c^2(t \pm z)} << 1 \tag{1.36}$$

and at angles from the axis greater than

$$\theta^2 \gtrsim \frac{4GM}{Rc^2}. \tag{1.37}$$

Thus, for any M there is also a lower bound on R (see fig. 1.4).

Upon making the coordinate transformation given by eq. (1.7), angles on the sphere will

1. In reality, quantum effects de-localize the photon. One could smooth out the singular behaviour using a Gaussian distribution (e.g. a coherent state), which would lead to finite curvature on the axis.

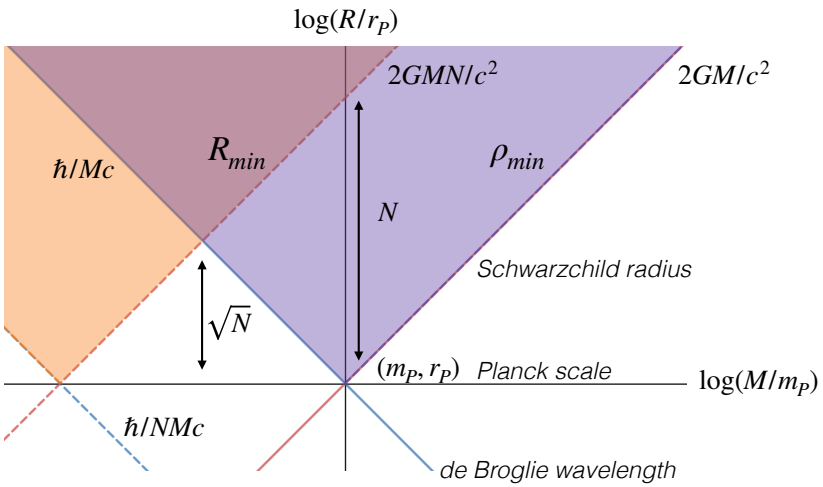

Figure 1.4: Shaded regions schematically show the range of validity for the spherical decay solution imposed by linearity of classical gravitational distortion at large M, and localization of quantum mass-energy of the decaying particle at small M. For a system of N particles, the boundaries are displaced as shown.

become distorted, i.e. $\theta \neq \tilde{\theta}$. However, one can show that the leading order difference satisfies

$$\cos\tilde{\theta} - \cos\theta \sim \frac{GM}{Rc^2} \ln\left(\frac{1+\cos\theta}{1-\cos\theta}\right) \tag{1.38}$$

So long as R is much larger than the Schwarzschild radius and we are not too close to the poles, we may use $\theta \approx \tilde{\theta}$ in all of our formulas since the displacement and velocity kicks are $\mathcal{O}(M/r)$, and the difference in angles will contribute at sub-leading order.

For many particles, the solution also requires R to be much larger than the Schwarzschild radius for the whole central mass. For N particles of mass M on the same world line, we require

$$R \gtrsim R_{min} = 2GNM/c^2; \tag{1.39}$$

otherwise, the sphere of clocks is inside the Schwarzschild radius of the mass, forming a black hole.

So far, we have considered only the limits of the classical solution. In a real physical system, the quantum properties of a point particle add other constraints. The mass-energy

of the particle is delocalized in space and time by an amount that depends on the character of its quantum state. For example, the de Broglie wavelength, $\lambda_M = \hbar/Mc$, gives the minimum spatial uncertainty of position for a massive particle that is localized in time. This value is shown in fig. 1.4.

In the classical solution, the source is a single pointlike object with a definite trajectory. In quantum reality, it is a single quantum object whose wave function in space depends on its localization in time. Temporal coherence leads to correlations that are nonlocal in proper time, which affects the coherence of the metric distortion in the timelike direction.

The wave packet of particle location spreads out in space and time. The minimum spatial width of a location wave function for a measurement of duration τ, or "standard quantum uncertainty" [Caves, 1980a,b], is given by

$$\langle \Delta x^2 \rangle > \hbar\tau/NM \tag{1.40}$$

for a state of total mass NM. On the surface of a causal diamond with $R = c\tau$, the spatial uncertainty in the central world line leads to an angular quantum uncertainty,

$$\langle \Delta\Theta^2 \rangle \sim \langle \Delta x^2 \rangle / R^2 \ \sim (c\tau/R)(\hbar/NMc)R^{-1} \ > \ \hbar/NMcR. \tag{1.41}$$

Thus, the quantum bounds become important when both M and R are small. fig. 1.4 shows the range of classical and quantum validity in Planck units:

$$m_P \equiv \sqrt{\hbar c/G}, \quad r_P \equiv ct_P \equiv \sqrt{\hbar G/c^3} = \hbar/m_P c. \tag{1.42}$$

1.7 Quantum Superpositions

1.7.1 Quantum Superposition of Randomly Oriented Decays

In the region of validity shown in fig. 1.4, the calculation far from the polar axis is a good approximation for both general relativity and quantum mechanics. In that regime, it can be reliably extrapolated to consider quantum states of the nonlocalized metric of a causal diamond. The entire setup, including the geometry itself and the sphere of clocks used to measure it, can be treated as a coherent quantum system.

If a decaying particle is a quantum system, the quantum nonlocality of the "spooky" two-particle decay state also leads to a delocalized, Schrödinger-cat-like macroscopic superposition of space-times. As usual in quantum mechanics, there is no paradox: if the preparation of states is causal, the quantum coherence of the decaying-particle products entangles with the coherent causal diamonds of the distorted space-time, and the corresponding displacements of clocks.

Suppose the null particles from a decay are created in a quantum S-wave state, whose wave function is an isotropic superposition of all directions. This leads to a superposition of space-time distortion patterns. The wave function of the space-time includes a superposition of all the different orientations of the classical gravitational distortions, each one an eigenstate of the particle decay axis. Each metric in the superposition is coherent over a macroscopic causal diamond, starting with the decay and ending with the null incoming reflection from the boundary that carries the clock readings back to the observer. The wave function can be described as a sum of state amplitudes over histories, where the sum includes not just a world line, but a whole causal diamond. A measurement of a particle axis will always find itself with a causal-diamond history consistent with it.

The classical solution shows that fractional distortion Δ of time displacement, as measured by observed clocks, varies coherently on the causal diamond surface of radius R ac-

cording to eq. (1.25),

$$\Delta = \delta\tau/(R/c) = cT_2(\theta)/R \simeq \frac{5Mc}{24R}(3\cos^2\theta - 1) \tag{1.43}$$

The system with a single particle can be extrapolated by linear superposition to a system of many particles. If there are N decaying particles of mass M_i in the causal diamond, the large-angle coherence does not decrease from averaging their effects: instead, the amplitudes of their distortions linearly add. The coherent quantum state of time distortions on the sphere from N such decays on the same world line can be written as a sum

$$|\Delta(\theta,\phi)\rangle = \sum_{i=1}^{N} \alpha_i(\vec{n}_i)|\Delta(\theta,\phi)_i\rangle, \tag{1.44}$$

where each element of the sum represents a decay along a different random axis $\vec{n}_i$.

Each decay creates the same universal distortion pattern relative to its own axis. Their sum does not give a universal pattern, but it does give a universal power spectrum: the spherical harmonic distortion coefficients $\alpha_{\ell m}$ from each decay pattern $\Delta(\theta,\phi)_i$ add in quadrature. For example, for equal mass particles $M = M_i$, the quadrupolar variances add to give fluctuations with a total quadrupolar variance

$$\langle\Delta^2\rangle_2 = \sum_{m=-2}^{2}\sum_{i=1}^{N} \alpha_{2m}(i)^2 \sim N(GM/Rc^2)^2, \tag{1.45}$$

where $\alpha_{2m}(i)$ denote the quadrupolar amplitudes for each decay, derived above (see eq. (1.25)). Note that for a given total mass NM, the gravitational distortion decreases with N but increases with an adopted granularity scale M. This result depends only on standard physics, and a conservative application of the quantum correspondence principle, that the gravity of a quantum system is the same as that of an identical classical one.

The same estimate applies to large-angle gravitational distortions created by non-interacting

massless null particles that enter and leave the boundary of a volume with radius R. For a gas with with a mean occupation of N particles inside R, eq. (1.45) approximately gives the variance of large-angle gravitational fluctuations on the surface.

This framework is self-consistent until N is large enough that the gravity of the particles affects the mean curvature of the causal diamond. For consistency, in order not to form a black hole with radius less than R, we require

$$R < R_S = 2G(NM)/c^2 \tag{1.46}$$

so their number must not exceed

$$N_{max} \sim c^2 R/2GM. \tag{1.47}$$

For a gas of particles that saturates the bound $N = N_{max}$, the quadrupolar gravitational redshift distortion,

$$\langle \Delta^2 \rangle_2 \sim GM/2Rc^2, \tag{1.48}$$

decreases with R, which shows that a large system has a nearly-determinate, classical metric. Note that Planck's constant $\hbar$ does not appear in eq. (1.48): although it is a quantum uncertainty, based on superposition of multiple decays, its magnitude is determined by the assumed discreteness scale, M.

1.7.2 Coherent Quantum-Gravitational Fluctuations

For particle states confined to a volume of size R, extrapolation to N_{max} in eq. (1.48) gives an estimate of the gravitational fluctuations created by randomly-oriented particle states with a UV cutoff M. This applies approximately to the case of a system filled with particles whose density approximately saturates the bound, such as a cosmological solution or black

hole on the scale of the horizon. For a UV cutoff at the Planck scale $M = m_P$, eq. (1.48) with $R = c\tau$ becomes

$$\langle \Delta^2 \rangle_2 \sim \langle \delta\tau^2 \rangle / \tau^2 \sim t_P/\tau. \tag{1.49}$$

As expected, quantum-gravitational fluctuations are of the order of unity for τ at the Planck scale. The surprising feature of eq. (1.49) is the linear inverse dependence on τ for duration τ much longer than t_P. The gravitational effects of vacuum field fluctuations in effective field theory have long been studied in the context of inflationary universes (e.g., [Starobinsky, 1982, Weinberg, 2008b, Baumann, 2011]). In these systems, gravitational quantum uncertainty decreases as a higher power with scale: the typical relic metric fluctuation on the scale of an inflationary horizon of radius $c\tau$ is

$$\langle \Delta^2 \rangle_{EFT} \sim (t_P/\tau)^2. \tag{1.50}$$

The different results arise from different models of quantum coherence. The larger fluctuations in the decaying-particle system can be traced to the fact that a point particle creates a displacement that is coherent on scale $c\tau$ for a causal diamond of any duration τ. The coherence scale in the effective field system is that of the particle wave function, $\sim \hbar/Mc$, so the variance is reduced by a factor $\sim 1/\tau$. Our classical solution explicitly shows that the physical gravitational effect corresponds to the former case: the gravity of a point particle imprints a large-angle, quasi-tidal coherent geometrical structure on macroscopic scales, much larger than the de Broglie wavelength of the particle.

For causally-coherent gravity, the large-angle, macroscopic distortion actually increases with duration, with variance

$$\langle \delta\tau^2 \rangle_2 \sim \tau \; t_P. \tag{1.51}$$

This scaling behavior follows directly from the classical solution via eq. (1.45): the coherent large-angle memory of each Planck-energy single-particle state is independent of R, so the

total distortion grows with the duration in the same way as a random walk.

Our semiclassical treatment meshes well with previous arguments that suggest macroscopic coherence of geometrical quantum states. For physical field states not to exceed the black hole mass in any volume, gravity requires macroscopic nonlocal coherence in the infrared [Cohen et al., 1999, Banks and Draper, 2020, Cohen and Kaplan, 2021]. Nonlocally coherent geometrical states ("entanglement wedges") are also key elements in recent resolutions of the black hole information paradoxes, incorporated into an account of fine-grained entropy [Almheiri et al., 2020]. Formal methods based on conformal descriptions of near-horizon states show that coherence can produce physical metric distortions comparable in amplitude to those estimated here, both for black hole horizons and causal diamond surfaces in flat space-time [Zurek, 2020, Banks and Zurek, 2021].

The time distortions on the causal diamond surface can be continuously extrapolated to provide a physical heuristic picture of what happens when a black hole evaporates. As a black hole evaporates (or is assembled) one particle at a time, each particle maps onto a coherent, mostly quadrupolar distortion that extends across the entire horizon surface, of the order of one Planck length in amplitude. A long-lived horizon is a superposition of a sequence of many such distortions. This simple picture of coherent horizon distortions agrees with a "quantum-first" analysis of evaporation [Giddings, 2017, 2019]. In this view, states of Planck-scale "quantum foam" are wave functions coherently spread everywhere across the horizon, no matter how large it is.

1.8 Conclusion

The Schrödinger-cat-like states of space-times with quantum decaying particles— superpositions of different geometries with macroscopically distinguishable physical properties, such as quadrupole moments of observable time distortions— show concretely how quantum-gravitational coherence works. The quantum construction uses particle-like states of matter,

with superpositions of wave functions localized to causal diamonds, instead of quantized plane-wave states that extend to infinity, so it allows both preparation and measurement of states from a single world line. Directional indeterminacy of quantum states is reconciled with gravity via a conventional correspondence principle, leading to quantum-geometrical states that are directionally coherent on null surfaces. It explicitly shows nonlocal, anisotropic effects of gravitational coherence manifested in a local measurement.

Our analysis shows that macroscopic coherence of quantum gravity has concrete physical consequences. Coherence leads to quantum-gravitational distortions on large angles and macroscopic scales, with variance that grows linearly with duration. The smaller variation predicted by effective field theory does not account for the physical effects of directional causal coherence.

The anisotropic distortion of time is a real physical effect, not a gauge artifact: in principle, it can be measured with actual clocks or laser interferometers. The permanent time displacement between the observer's clock and any of the other clocks is an objective measurable quantity. Different states correspond to physically different geometries on macroscopic scales.

It is possible that the coherence of active quantum gravity could be measured not just in principle, but in an actual experiment. Although the distortions of physical black hole horizons are likely to be unobservable, a direct measurement of causal diamond distortions may be accessible to Michelson interferometers correlated to reveal spacelike coherence [Chou et al., 2017, Richardson et al., 2021]. The effect of coherent horizons would produce primordial perturbations during cosmic inflation of the order of eq. (1.49), much larger than standard inflation theory, and could create new causally-coherent symmetries of angular correlations in cosmic microwave background anisotropy. These symmetries appear to be consistent with anomalous correlations measured in the CMB on large angular scales [Hogan, 2019, 2020b, Hagimoto et al., 2020, Hogan and Meyer, 2021].

CHAPTER 2

GRAVITY OF GLUONIC FLUCTUATIONS

2.1 Introduction

A widely repeated calculation for the value of the cosmological constant, based on summing the zero point fluctuations of quantum fields, gives a famously wrong answer [Weinberg, 1989, Padmanabhan, 2003, Weinberg, 2008a]: the sum of zero-point mode-fluctuation energies up to a UV cutoff at mass scale M leads to a cosmological constant Λ equivalent to a mass density of order $\rho_\Lambda \sim M^4c^3/\hbar^3$, which leads to a gravitational cosmic acceleration rate of order $H_\Lambda \sim (M/m_P)^2/t_P$, or a cosmological constant

$$\Lambda \sim (M/m_P)^4/t_P^2, \tag{2.1}$$

where $t_P = \sqrt{\hbar G/c^5}$ denotes the Planck time. For M equal to the Planck mass $m_P = \sqrt{\hbar c/G}$, the predicted value of Λ is larger than the observed value by about 122 orders of magnitude. Experiments [Adelberger et al., 2009, Kapner et al., 2007] rule out proposed modifications of gravity or quantum field fluctuation amplitudes with a cutoff at the milli-eV mass scale that would give the correct value of Λ.

For this reason, it is widely agreed that there must be a basic conceptual error in the way this calculation is formulated. There needs to be a basic symmetry of quantum gravity that makes the gravitation of vacuum field fluctuations nearly vanish, and also a mechanism to account for the nonzero measured value of the actual cosmological constant.

One possibility is that symmetries of quantum geometry make Λ exactly vanish for point-like particles, but allow a small nonzero Λ from the gravity of nonlocal vacuum fluctuation states of interacting fields. In this case, the value of ρ_Λ would be much less than the Planck value quoted above, suppressed by a power of the field energy scale. A long-studied example is the hypothesis [Zel'Dovich, 1967, Zeldovich, 1968, Schutzhold, 2002, Bjorken, 2003,

Brodsky and Shrock, 2011, Bjorken, 2010, Klinkhamer and Volovik, 2009, Poplawski, 1990, Hogan, 2020a] is that the cosmological constant arises from quantum fluctuations in the strong interaction vacuum.

Studies of this hypothesis have generally sought to compute the expected low-energy energy momentum tensor from the system of QCD quantum fields. In this paper, we instead analyze the system geometrically, using classical gravitational models. We estimate the gravitational effect of QCD field fluctuations by analyzing simple idealized classical systems whose energy-momentum structure resembles that of pions, the lowest-energy QCD excitations. The energy-momentum of these systems is dominated by the kinetic energy of pointlike quarks and massless gluons, and the nonlocal self-attractive interaction of the gluons. We then use these systems to estimate the coherent quantum-gravitational effects of pion-like vacuum fluctuations in causal diamonds, and show that they approximately agree with the measured cosmic acceleration.

In our simple models, fluctuations of gluonic tension produce secular repulsive gravitation. The energy-momentum tensor of a homogeneous condensate of massless gluons in localized virtual fluctuations takes a form proportional to the metric, with pressure and density related by $p = -\rho c^2$ in one or more dimensions. For more than one dimension, this equation of state violates the strong energy condition, so its gravitational effect is repulsive. In field language, this behavior for gluonic fluctuations in strongly-interacting QCD vacua arises from the gravitational effect of a trace anomaly [Schutzhold, 2002]. The one-dimensional case is also familiar from early models of pions which modeled strong interactions as strings.

Like early phenomenological models of hadrons (e.g. Andersson et al. [1983]), our analysis does not provide a rigorous connection to QCD field degrees of freedom. However, it provides a simple classical model for gravitational effects of nonlinear QCD fluctuations, and shows how they depend critically on nonlocal causal coherence of field states in more than one dimension. It provides physical insights into how the gravity of vacuum fluctuations works at

a microscopic level, in particular the reason for the small value of the cosmological constant. Simply put, the model shows that *if quantum degrees of freedom of gravity are coherent in causal diamonds, cosmic acceleration from quantum fluctuations of QCD has about the same magnitude (with opposite sign) as Newtonian gravitational acceleration at the edge of a proton.*

2.2 Causally Coherent Gravity of Gluonic Fluctuations

We study the dynamics and gravity of two idealized models with different geometries. The first model, shown in fig. 2.1, is a bubble: a spherical volume of gluonic matter is approximated by a uniform isotropic tension and density with the locally Lorentz-invariant relationship

$$p = -\rho c^2 \tag{2.2}$$

in three dimensions, bounded by a uniform shell of dustlike quark material of constant total mass. The other model, discussed in section 2.5, is a more traditional idealized model of pions, where a straight gluonic string with $p = -\rho c^2$ in one dimension joins two light pointlike quarks. The two systems have similar dynamics: they start at small radius with a large γ factor, expand to a maximum size determined by the masses of the quarks and the tension of the gluons, then recollapse.

We do not provide a derivation that this equation of state is the correct one for QCD vacuum fluctuations, but point out that *any* homogeneous vacuum state must be locally Lorentz invariant, so its mean energy-momentum tensor must transform like the metric: $T_{ab} = -\rho g_{ab}$. Our model demonstrates that if fluctuations of stress-energy are confined to compact causal diamonds with this equation of state and a size and total mass equal to that of the pion, it produces a global relative acceleration between neighboring test bodies consistent with that of the cosmological constant.

As discussed below, tension in more than one dimension is required for gravity to produce cosmic acceleration, so we focus on the bubble model. Since it is spherically symmetric, gravity outside the bubble is simply a Schwarzschild metric. Inside the bubble, the effect of the quarks on a test particle resembles displacements by a null shock on a causal diamond, whose outwards and inwards gravitational displacements cancel over a whole orbit. The main gravitational effect in the interior is from the gluonic matter.

We find that gravity inside the bubble produces a mean repulsive residual velocity, in the sense that on average it causes test particles within the orbit to accelerate systematically apart from each other in the radial direction. Ultimately this unique behavior can be traced to the exotic nature of the source, whose mass-energy, dominated for much of its orbit by the gluonic matter with $p = -\rho c^2$, violates the strong energy condition. (The string model, which does not violate this condition, also creates repulsive gravitational impulses along some directions, but not in a global average.)

We then adapt the classical model to estimate the mean gravitational effect of QCD vacuum fluctuations. Gravitationally repulsive virtual gluonic material is borrowed from vacuum, so its gravitational effect only extends over a compact causal diamond with a radius $\sim \hbar/m_\pi c$ determined by the pion mass m_π. Since all of space in a sense lies "inside a virtual bubble", this model leads to a simple picture of how cosmic repulsion works. Within the causal diamond of a fluctuating bubble, test bodies on one side of the bubble accelerate away from the center, and if quantum gravity is causally coherent, also away from the entire future light cone beyond the center. The acceleration is approximately the Newtonian gravitational acceleration for a mass with the bubble density and bubble radius, rather than a cosmic radius. As discussed further below, virtual bubbles thus create gravitational fluctuations whose secular gravitational repulsion is much smaller than eq. (2.1):

$$\Lambda \sim (m_\pi/m_P)^6/t_P^2. \tag{2.3}$$

As shown below, the bubble estimate approximately agrees with the measured cosmological constant for parameters similar to physical pions: for mass $M = m_\pi$, it requires a bubble radius $R_0 \sim 2.0\ \hbar/m_\pi c$, about two femtometers. Such close agreement is remarkable, since the model is idealized in several important ways. For example, a smaller radius would be expected from the fact that real QCD fluctuations do not have a maximally-repulsive isotropic equation of state; their gravity would be expected to behave like something in between the bubble and the string.

The model provides a well controlled connection, albeit still idealized, between the measured properties of pions and the measured cosmological constant. The rather close agreement, based on a simple correspondence argument and a highly idealized model system, suggests that if gravitational states of the field vacuum are coherent in causal diamonds, an absolute value for the cosmological constant can in principle be derived from properties of Standard Model fields. Realistic numerical studies of gravitational effects from the QCD vacuum would not require a theory of quantum gravity, but would require a coherent nonlocal calculation of expected mass-energy flows in the vacuum state.

2.3 Gluonic Bubble Model

2.3.1 Bubble Model with Light Quarks

The idealized "gluonic bubble" model (fig. 2.1) is a spherical ball of total mass M, filled with uniform gluon gas of the unique Lorentz-invariant form $p_0 = -\rho_0 c^2$, surrounded by a thin sheet of pressureless quark dust of total mass m on the surface. It captures the nonlocal, nonabelian self-tension of the gluon fields in an idealized way that complements the 1D string model more commonly used for pions. It allows for a solution of the Einstein equations and derivation of gravitational effects for an isotropic pressure in 3D. We call it a bubble model to differentiate from the bag model, an idealized picture of a stable nucleon

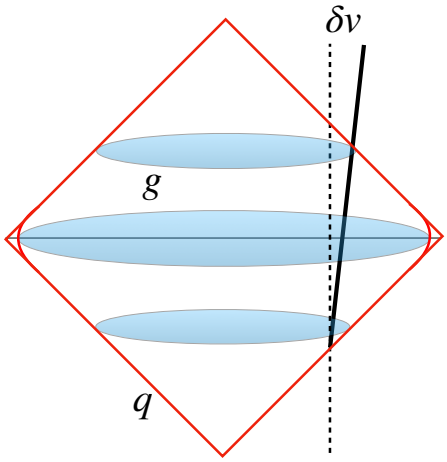

Figure 2.1: Spacetime diagram of the gluonic bubble model. The diamond represents a bubble of total mass M filled with gluonic material g with $p = -\rho c^2$ and gravitational timescale T_0, with a spherical quark shell q of mass $m << M$ on a nearly-null trajectory. The shell first propagates outwards to maximum radius R_0, then collapses inwards, separated by a small nonrelativistic reversal region. The timelike world line represents a freely falling body. The gravity of the gluonic matter produces an outwards residual velocity $\delta v_g \sim +R_0^2/cT_0^2$ during the time a body spends within the bubble (eq. (2.9)).

in a confining vacuum. The bubble model, like the string model, is an idealized picture of the dynamical mass-energy of QCD fields in a pion-like state, designed to approximate the virtual fluctuating energy flows of the QCD vacuum.

The quarklike surface of the bubble is dust, that is, it has no tension or pressure, and is infinitesimally thin. Its mass is constant as it expands, so the mass density thins out, and the inwards acceleration from the constant gluonic tension increases. The equation of motion is thus not the same as the string model, but the solutions are similar. For light quarks $m << M$, the bulk of the orbit is relativistic inwards or outwards motion. There is a brief turnaround near maximum expansion where the velocities are much less than c.

2.3.2 Residual Velocity From a Bubble Orbit with Light Quarks

In the bubble model, there is no gravitational radiation, so the outgoing and incoming parts of the orbit are identical under time reversal. The inwards and outwards shocks from the

passage of the quark surface identically cancel, so there is no residual gravitational effect of the quark surface on the motion of test particles, apart from those of a "background" Schwarzschild solution of mass M, which is the space-time outside the bubble.

However, worldlines that pass through the interior of the bubble's causal diamond accumulate outwards acceleration while they are inside. The mean gravitational effect on test bodies during the time that they pass within the volume of the bubble leaves behind an outwards "residual velocity" whose mean cumulative effect resembles cosmic acceleration.

It is a well known result in general relativity that the gravitational acceleration at radius r relative to the center of a homogeneous sphere is

$$a(r) = \dot{v} = -(4\pi/3)Gr(\rho + 3p/c^2). \tag{2.4}$$

This Newtonian weak field limit is valid for a system much smaller than the Schwarzschild radius of the contained mass. For empty space outside the sphere, the solution is Schwarzschild so it approaches flat space at large radii. In the opposite limit where matter uniformly fills a large volume, the exact solutions are FRW cosmologies.

The effect of general relativity is captured by the last term, the Newtonian gravitational effect of pressure. The large negative pressure within the volume of a gluon bubble leads to a net positive acceleration or gravitational repulsion at radius r,

$$a_g(r) = \dot{v} = +r/T_0^2, \tag{2.5}$$

where we have defined a gravitational timescale

$$T_0 \equiv (8\pi G\rho_0/3)^{-1/2}, \tag{2.6}$$

for a gluonic bubble of maximum radius R_0 and density

$$\rho_0 = (M - m)(4\pi R_0^3/3)^{-1}. \tag{2.7}$$

In the light quark limit $m << M$, we can ignore the short turnaround part of the orbit. A worldline at radius r spends a time $\tau_g(r) = 2(R_0 - r)/c$ inside the bubble. The outward velocity accumulated at radius r during this time is

$$\delta v(r)_g = \tau_g(r) a(r)_g = +2r(R_0 - r)/cT_0^2 \tag{2.8}$$

This quantity vanishes both at $r = R_0$ and $r = 0$, so there is no residual velocity kick for a world line on the maximal boundary of the bubble or at the origin. In between, the residual velocity is positive, with a maximum value at $r = R_0/2$,

$$\delta v_g(r = R_0/2) = +R_0^2/cT_0^2. \tag{2.9}$$

After a bubble orbit, two particles on opposite sides of the center are moving apart by the sum of their two kicks. Several sample trajectories are shown in fig. 2.2.

In the classical solution, this outwards velocity kick is combined with an inwards acceleration accumulated while a world line lies outside the bubble, where the metric is a Schwarzschild solution of mass M. The source in this regime includes the gravity of the (mostly relativistic) quark material as well as the total mass of the gluonic material. As noted above, the quark contribution vanishes in the limit of light quarks, since the inwards and outwards shocks cancel.

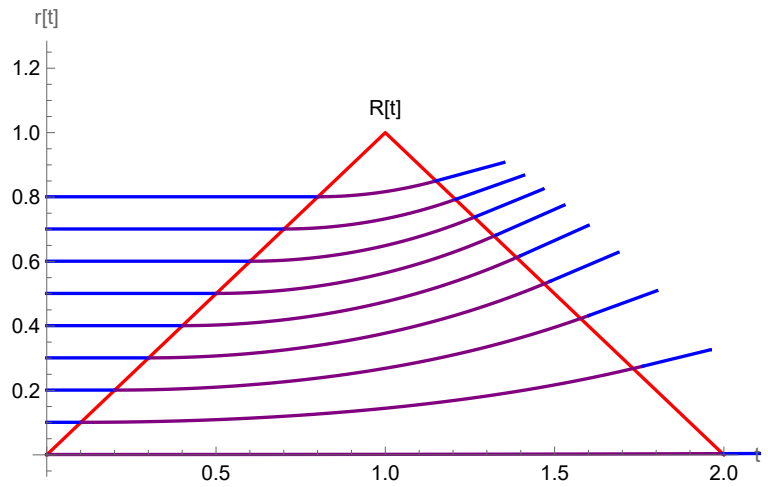

Figure 2.2: Trajectories of test particles (blue/purple) accelerating within the causal diamond (red) of a bubble with $m << M$ and $R_0 = 1$, according to eq. (2.5). The acceleration increases with increasing r, but the total time inside the bubble decreases with increasing r, so the maximum residual velocity eq. (2.8) occurs at $r = R_0/2$. For illustration, the motion of the test particles is exaggerated in this plot by a factor of R_0^2/T_0^2 compared to that of the bubble wall, or about 40 orders of magnitude for QCD fluctuations.

2.3.3 Gluonic Bubble Solution for $m \neq 0$

To rigorously solve for the dynamics of the bubble, we will apply the Israel junction conditions following Barrabès and Israel [1991]. We will begin by considering gluing two general spacetimes, then restrict ourselves to the spherically symmetric case, and finally further restrict to the weak field regime (still allowing for the possibility of relativistic velocities). In this section we work in units where $c = 1$ to avoid keeping track of factors of c when raising and lowering tensor indices with the metric. Consider two distinct spacetime manifolds $\mathcal{M}_+, \mathcal{M}_-$ with associated metrics $g^+_{\alpha\beta}(x^\mu_+), g^-_{\alpha\beta}(x^\mu_-)$. The two spacetimes are bounded by hypersurfaces Σ_+, Σ_- with induced metrics g^+_{ab}, g^-_{ab} $(a, b = 1, 2, 3)$. We can glue the spacetimes together by making the identification $\Sigma_+ = \Sigma_- = \Sigma$ with intrinsic coordinates ξ^a.

We can construct a tetrad of vectors $n^\mu, e^\mu_{(a)}$ $(\mu = 0, 1, 2, 3)$ (which can be defined in

both spacetime regions) satisfying

$$n_\mu n^\mu|_+ = n_\mu n^\mu\big|_- = 1 \quad , \quad n_\mu e^\mu_{(a)}\Big|_\pm = 0 \tag{2.10}$$

where the vectors $e^\mu_{(a)}$ are adapted to the hypersurface Σ such that

$$g^\pm_{ab} = g_{\alpha\beta}\, e^\alpha_{(a)} e^\beta_{(b)}\Big|_\pm \tag{2.11}$$

We can parametrically define Σ such that $\Phi \equiv R(t) - r = 0$ on the hypersurface. This gives a natural identification of hypersurfaces of $\Phi > 0$ with $\mathcal{M}_+$ and hypersurfaces of $\Phi < 0$ with $\mathcal{M}_-$. We can then define n^μ to be normal to surfaces of constant Φ such that $n_\mu = \alpha^{-1}\partial_\mu \Phi$, where α is chosen to ensure normalization.

One can show that by appropriate choice of intrinsic coordinates ξ^a we can make $g^+_{ab}(\xi) = g^-_{ab}(\xi) = g_{ab}(\xi)$. However, there will be a discontinuous jump in the normal extrinsic curvature defined by

$$K_{ab} = -n_\mu e^\nu_{(b)} \nabla_\nu e^\mu_{(a)} \tag{2.12}$$

In Newtonian gravity, this gives rise to the familiar jump in the normal derivative of the Newtonian potential. The induced surface stress-energy can be related to the jump in the extrinsic curvature by an analog of the Einstein equations

$$-8\pi \left(S_{ab} - \frac{1}{2} g_{ab} S \right) = [K_{ab}] \tag{2.13}$$

where $[F]$ denotes $(F_+ - F_-)\,|_\Sigma$, i.e. the difference in F across the hypersurface Σ. The full stress-energy tensor restricted to the hypersurface Σ is then given by

$$T^{\mu\nu}_\Sigma = -S^{ab} e^\mu_{(a)} e^\nu_{(b)} |\alpha| \delta(\Phi) \tag{2.14}$$

Now, we will restrict our attention to spherically symmetric spacetimes. In Eddington-Finkelstein coordinates, the metric can be written as

$$ds^2 = e^{\psi} du(f e^{\psi} du + 2\zeta dr) + r^2 d\Omega \tag{2.15}$$

where $u = t - \zeta r^*, dr^*/dr = 1/f$ and $f(u,r) = 1 - 2m(u,r)/r$. $\zeta = \pm 1$ denotes whether the hypersurface Σ is moving outward (increasing r) or inward. The Einstein equations then give us differential equations for the functions m, ψ.

$$\partial_u m = 4\pi r^2 T^r_u \tag{2.16}$$

$$\partial_r m = -4\pi r^2 T^u_u \tag{2.17}$$

$$\partial_r \psi = 4\pi r T_{rr} \tag{2.18}$$

For the bubble model being considered, the stress-energy inside of the shell is that of a de-Sitter spacetime with positive cosmological constant and stress-energy proportional to the spacetime metric.

$$T^{dS}_{\mu\nu} = -\rho g_{\mu\nu} \tag{2.19}$$

In the Eddington-Finkelstein coordinates we find

$$T^u_u = T^r_r = T^\theta_\theta = T^\phi_\phi = -\rho \tag{2.20}$$

Therefore we get that $T_{rr} = 0, T^r_u = 0$, which by eq. (2.18),(2.16) imply $\psi = 0, f = f(r)$. Solving eq. (2.17) assuming the exterior region to be Schwarzschild, we find

$$f_+ = 1 - \frac{8\pi}{3}\rho r^2 \tag{2.21}$$

$$f_- = 1 - \frac{2M}{r} \tag{2.22}$$

Now we may explicitly define the tetrad in terms of the chosen coordinates. We will switch back to using the more familiar t, r coordinates.

$$n_\mu = -\frac{1}{(f - f^{-1}\dot{R}^2)^{1/2}} \left(\delta^r_\mu + \dot{R}\delta^t_\mu\right) \tag{2.23}$$

where the over-dot signifies the derivative with respect to coordinate time t. The intrinsic metric for the timelike spherical shell is given by

$$ds^2_\Sigma = -d\lambda^2 + r^2 d\Omega^2 \tag{2.24}$$

where λ is the proper time of a co-moving observer on the shell. Then we can choose the rest of our tetrad vectors to be

$$e^\mu_{(1)} = \frac{1}{(f - f^{-1}\dot{R}^2)^{1/2}} \left(\delta^\mu_t + \dot{R}\delta^{\mu r}\right) \tag{2.25}$$

$$e^\mu_{(2)} = \delta^\mu_\theta \tag{2.26}$$

$$e^\mu_{(3)} = \delta^\mu_\phi \tag{2.27}$$

One can compute the extrinsic curvature using eq. (2.12), which produces the following stress-energy on the spherical shell:

$$-S^{ab} = \sigma\delta^a_1\delta^b_1 \tag{2.28}$$

$$T^{\mu\nu}_\Sigma = |\alpha|\sigma e^\mu_{(1)} e^\nu_{(1)} \delta(r - R(t)) \tag{2.29}$$

where σ is the surface energy density of the shell given by

$$\sigma = -\zeta\frac{[m]}{4\pi r^2} \tag{2.30}$$

The form of eq. (2.29) is that of a pressureless dust in the rest frame of the shell. In the weak-field limit this reduces to the usual form

$$T_{\Sigma}^{\mu\nu} \approx \frac{\gamma m}{4\pi r^2} v^{\mu} v^{\nu} \delta(r - R(t)) \tag{2.31}$$

where $v^{\mu} = dx^{\mu}/dt, \gamma = (1 - \dot{R}^2)^{-1/2}$. The evolution of the shell radius $R(t)$ is determined by conservation of stress-energy and is given by

$$\left[\mathrm{sgn}(n^{\nu}\partial_{\mu} r)(f + (dR/d\lambda)^2)^{1/2}\right] = -\frac{M}{r} \tag{2.32}$$

Using the definition for n^{μ} and $f_{\pm}$ we find

$$\Gamma m = M - \frac{4}{3}\pi r^3 \rho \tag{2.33}$$

where Γ is defined by

$$2\Gamma = (f_{+} + (dR/d\lambda)^2)^{1/2} + (f_{-} + (dR/d\lambda)^2)^{1/2} \tag{2.34}$$

In the weak field limit with $dR/d\lambda >> 1$ this reduces to

$$\Gamma \approx \gamma = (1 - \dot{R}^2)^{-1/2} \tag{2.35}$$

which is consistent with the expected mass/energy conservation law.

Next, let us define the glued metric over the entire spacetime by

$$\tilde{g}_{\mu\nu} = g_{\mu\nu}^{+}\Theta(\Phi) + g_{\mu\nu}^{-}\Theta(-\Phi) \tag{2.36}$$

where $\Theta(x)$ is the Heaviside step function, and Φ again parameterizes the hypersurface Σ.

Other quantities with an over tilde are defined to have a similar meaning. Since the metric can be made continuous along Σ, we get

$$\begin{aligned}\partial_\alpha \tilde{g}_{\mu\nu} &= \partial_\alpha g^+_{\mu\nu}\theta(\Phi) + \partial_\alpha g^-_{\mu\nu}\theta(-\Phi) + [g_{\mu\nu}]\delta(\Phi)\partial_\alpha\Phi \\ &= \widetilde{\partial_\alpha g_{\mu\nu}}\end{aligned} \tag{2.37}$$

A direct consequence of eq. (2.37) is that the Christoffel symbols suffer a step discontinuity, but there is no $\delta(\Phi)$ contribution. Therefore, the radial acceleration experience by an observer crossing the shell does not produce an instantaneous displacement kick.

However, the Riemann tensor does contain such a delta function contribution, indicating that two nearby test bodies would experience an instantaneous relative velocity kick.

$$R^\alpha{}_{\beta\mu\nu} = \tilde{R}^\alpha{}_{\beta\mu\nu} - 2[\Gamma^\alpha_{\beta[\mu}]n_{\nu]}\alpha\delta(\Phi) \tag{2.38}$$

From this point forward we shall operate in the weak-field limit exclusively and assume $\gamma >> 1, m << M$. The full stress-energy tensor for a gluonic bubble connected to a shell of mass $m > 0$ is given by eq. (2.19) and (2.31)

$$T_{\mu\nu} = -\rho g_{\mu\nu}\Theta(R(t) - r) + \frac{\gamma m}{4\pi R(t)^2}\delta(r - R(t))v_\mu v_\nu \tag{2.39}$$

where ρ is the energy density of the gluonic region which acts as a perfect fluid with $p = -\rho$ and $v_\mu = (-1, \dot{R}, 0, 0)$ is the four velocity of the shell. Conservation of stress-energy gives the equation of motion for the surface of the bubble:

$$\ddot{R} = -\frac{4\pi\rho R(t)^2}{m\gamma^3} \tag{2.40}$$

This still assumes the bubble is small so the gravitational effect on the wall is negligible

compared to the gluon tension.

Finding a closed-form analytic solution to this differential equation is quite difficult. It is easier to find an approximate solution for $\gamma(t)$ during the initial era and the turn-around. The total mass of the system is conserved and is given by

$$M = \frac{4}{3}\pi\rho R(t)^3 + \gamma m \tag{2.41}$$

For highly relativistic initial velocity, we have $\dot{R} \approx 1, R(t) \approx t$. During this portion of the evolution, we have

$$\gamma(t) \approx \gamma_0 - \frac{4}{3m}\pi\rho t^3 \tag{2.42}$$

Near the turn-around point, the shell will become sub-relativistic. The equation of motion then approximates to

$$\ddot{R} \approx -\frac{4\pi\rho R_0^2}{m} \tag{2.43}$$

where R_0 is the maximum value of R at the turn-around. The solution is

$$R(t) \approx R_0 - \frac{2\pi\rho R_0^2}{m}(t - t_0)^2 \tag{2.44}$$

$$\gamma(t) \approx 1 + \frac{8\pi^2\rho^2 R_0^4}{m^2}(t - t_0)^2 \tag{2.45}$$

where $R(t_0) = R_0$. Before the turnaround, both $R(t), \gamma(t)$ are monotonic functions of time, so we can smoothly connect the cubic and quadratic regions for $\gamma(t)$. Numerical solutions to eq. (2.40) are plotted in Fig. 2.3. The corresponding boost factor γ is plotted in fig. 2.4.

In the limit of zero quark mass, the period of a single orbit of the bubble is given by $T = 2R_0$. For a test body which begins at rest at position r, the time spent inside of the bubble interior in the zero quark mass limit is given by $\tau = 2(R_0 - r)$. For the case

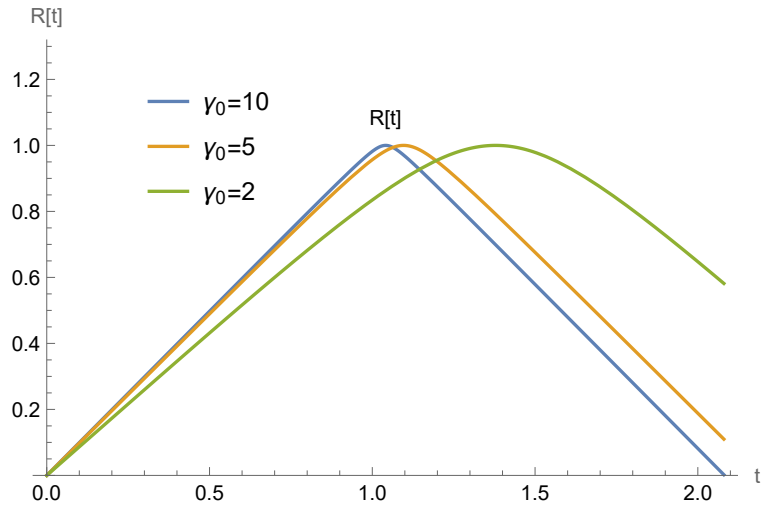

Figure 2.3: Trajectory of the shell $R(t)$ (solution to eq. (2.40)) for fixed bubble tension and variable initial boost factor γ_0. For $\gamma_0 \sim 1$, the trajectory is no longer predominantly nearly null, and the turnaround is less abrupt. The units of the spatial axis have been re-scaled by $\hbar/Mc$ while the units of the time axis have been re-scaled by $\hbar/Mc^2$.

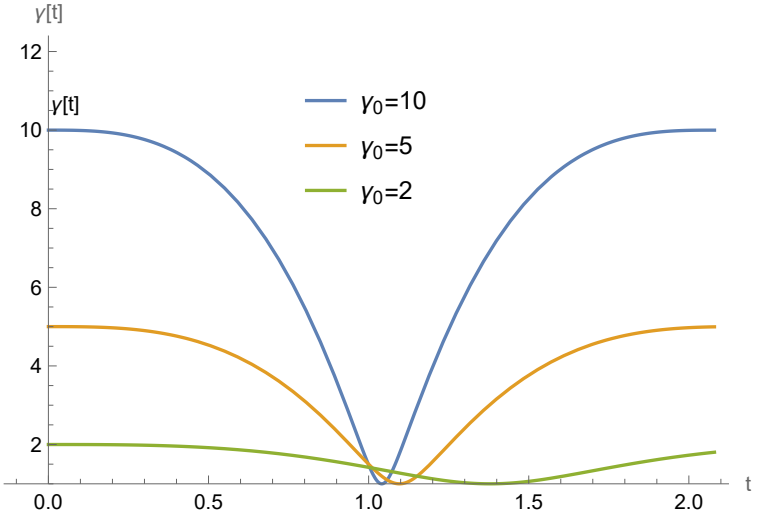

Figure 2.4: γ boost factor $\gamma = (1 - \dot{R}^2)^{-1/2}$ of the shell for fixed bubble tension and variable initial boost factor γ_0. The early and late time behavior are approximated in eq. (2.42) and (2.45).

$0 \neq m << M$, the period is given by

$$T = 2\int_0^{R_0} \frac{dR}{|\dot{R}|} \tag{2.46}$$

where $\frac{4}{3}\pi\rho R_0^3 = M - m$. From eq. (2.41) we find that

$$\dot{R} = \pm\left(1 - \frac{m^2}{(M - (4/3)\pi\rho R^3)^2}\right)^{1/2} \tag{2.47}$$

Plugging this into eq. (2.46), making a variable substitution, and substituting $\gamma_0 = M/m$ we get

$$T = 2R_0\int_0^1 \left(1 - \frac{1}{\gamma_0^2(1-(1-\gamma_0^{-1})x^3)^2}\right)^{-1/2} dx \tag{2.48}$$

Taylor expanding for $\gamma_0 >> 1$ the orbit period is approximately

$$T \approx 2R_0\left(1 + \frac{1}{3\gamma_0} + \frac{1}{27\gamma_0^2}(\sqrt{3}\pi + 9\ln 3 + 6\ln\gamma_0)\right) \tag{2.49}$$

The time spent inside of the bubble by a test body to leading order in m/M is given by

$$\tau \approx 2(R_0 - r)\left(1 + \frac{m}{3M}\right) \tag{2.50}$$

Meanwhile, the radial acceleration experienced by a test body scales as

$$\dot{v} = \frac{2M}{R_0^3}\left(1 - \frac{m}{M}\right) \tag{2.51}$$

Therefore the accumulated residual velocity after a single orbit is given by

$$\delta v \approx \frac{4M}{R_0^3} r(R_0 - r)\left(1 - \frac{2m}{3M}\right) \tag{2.52}$$

Since the true quark masses would yield $\gamma_0 \sim 10$, there will be a small but finite correction to

the estimate for the radius of the bubble needed to produce the observed cosmic acceleration computed in section 2.4.2.

2.4 Cosmic Acceleration

2.4.1 Gravity of Virtual Fluctuations

In our model of the gravitational effect of the vacuum, we will assume that virtual point particles have no gravitational mass. The whole gravitational effect of virtual QCD fluctuations lies within bubbles, and is dominated by gluons. Since a virtual fluctuation has zero mean energy and "borrows" energy only causally, the only gravitational effect is internal to the causal diamond occupied by the gluonic field fluctuation [Brodsky and Shrock, 2011]. Thus, nonlocal gluonic fluctuations produce a residual velocity between particles approximated by the classical bubble solution, given by eq. (2.9) for each fluctuation on scale R_0.

Consider gravitational repulsion from a space-filling vacuum of virtual pion-like bubbles as a model for how the physical cosmological constant is produced by QCD vacuum fluctuations. A small secular acceleration comes from the accumulation of small mutually repulsive velocity kicks within each orbit. The characteristic acceleration time is

$$T_\Lambda = R_0/\delta v_g \sim cT_0^2/R_0, \tag{2.53}$$

that is, it is larger than the gravitational timescale T_0 by a factor cT_0/R_0. In Planck units, $T_0^2 \sim M^{-4}$ and $R_0 \sim M^{-1}$, which leads to a "cosmic" acceleration rate

$$T_\Lambda^{-1} \sim M^3. \tag{2.54}$$

This approximately agrees with the observed value of Λ. As explained in more detail below, it is much smaller than the value that would correspond to a universe filled with gluonic

plasma of density ρ_0, or with thermal or quantum field excitations on the same scale, which is the standard estimate as in eq. (2.1),

$$T_0^{-1} \sim M^2. \tag{2.55}$$

The difference between the residual effect of a fluctuation, and the residual effect of a volume uniformly filled with the same material, arises because the gravitational acceleration from fluctuations comes only from the mass of material on the bubble scale R_0, instead of a volume with a gravitational radius $\sim cT_0$.

In this microscopic physical picture of how cosmic acceleration works, test particle trajectories, which are shown in fig. 2.2 in flat-space coordinates, correspond to geodesics of the emergent, slightly curved cosmological metric.

2.4.2 Cosmic Acceleration From Virtual Bubbles

The bubble model allows a more precise comparison of virtual bubble parameters with measured cosmic acceleration. Fits to cosmological dataTanabashi et al. [2018], Prat et al. [2022] yield an estimated value Λ_0 that corresponds to acceleration on a cosmic scale with a rate

$$T_\Lambda^{-1} \equiv \sqrt{\frac{\Lambda}{3}} = 1.0 \times 10^{-61}\ t_P^{-1}\ \sqrt{\frac{\Lambda}{\Lambda_0}}. \tag{2.56}$$

(A pure-vacuum cosmology would have a Hubble radius and event horizon radius $c/H_\Lambda = cT_\Lambda$.) We now evaluate the bubble parameters for which this mean cosmic acceleration matches the mean repulsive acceleration of test particles in the bubble model.

For virtual fluctuation states coherent on causal diamonds, the physical picture is that a test particle inside any virtual bubble accelerates away from the entire universe on the opposite side of the bubble's center at the mean rate given by the bubble model. The mean acceleration is given by the mean repulsive velocity impulse over a bubble orbit (eq. (2.8)),

divided by the duration of the orbit $2R_0/c$, which we equate with cosmic acceleration:

$$T_\Lambda^{-1} = (1/2)\langle \delta v_g/R_0 \rangle_B, \tag{2.57}$$

where $\langle\rangle_B$ denotes a volume average over the world lines that pass through the bubble. Since the impulse accounts for a whole orbit, an average that gives equal weight to each element of the bubble 3-volume also accounts for the time average of the fluctuating acceleration:

$$\langle \delta v_g(r) \rangle_B = \frac{\int_0^{R_0} dr r^2 \delta v_g(r)}{\int_0^{R_0} dr r^2} \tag{2.58}$$

This weighting yields

$$T_\Lambda^{-1} = 3R_0/20cT_0^2, \tag{2.59}$$

so writing the result in Planck units,

$$T_0^{-2} \equiv 8\pi G\rho_0/3 = 2M^4(R_0M)^{-3}, \tag{2.60}$$

we obtain

$$T_\Lambda^{-1} = (3/10)M^3(R_0M)^{-2}. \tag{2.61}$$

Apart from the numerical coefficient, with $R_0M \sim 1$ this is the same result as the simple estimate in eq. (2.54).

As a brief aside, we address a potential ambiguity in the averaging done in eq. (2.58). It may appear at first that since we are treating a single bubble with a center of mass, there is a preferred origin and the direction of acceleration averages to zero over the volume. However, this is merely an artifact of the fact that we have chosen to work in the coordinate description. If we analyze the geodesic deviation equation, we find that all nearby geodesics experience a uniform (coordinate independent) relative repulsion while passing through the

orbit of the bubble. If two nearby geodesics are initially separated by D^a, then their relative separation over time is given by eq. (9)

$$\frac{d^2 D^a}{dt^2} = \frac{8\pi\rho}{3} D^a \tag{2.62}$$

If one measures the acceleration of proper distance, we find that no form of spatial averaging can eliminate the acceleration between nearby test bodies. See appendix B. for more details.

Combining these results, the predicted cosmological constant from virtual gluonic bubbles in Planck units is:

$$\Lambda_{bubble} = 3\mathcal{H}^2 M^6, \tag{2.63}$$

where

$$\mathcal{H} \equiv (3/10)(R_0 M)^{-2}. \tag{2.64}$$

For bubbles with the physical pion mass ($M = m_{\pi_0} = 135\text{MeV}$), we find

$$\frac{\Lambda_{bubble}(M = m_\pi)}{\Lambda_0} = \left(\frac{R_0 m_\pi c}{2.0\ \hbar}\right)^{-4}. \tag{2.65}$$

That is, for pion-mass fluctuations to give the right cosmological constant, the one parameter in this simple model— the size of a bubble in units of the de Broglie wavelength for its mass— needs to be

$$R_0 = 2.0\ \hbar/m_\pi c, \tag{2.66}$$

for their mean gravity to produce the observed cosmic acceleration. This idealized model shows quantitatively how a cosmological constant close to the observed value results from the gravitational effect of vacuum fluctuations in QCD fields, as long as the quantum states of the fields and their gravity are coherent on causal diamonds.

2.4.3 Improvements on the Idealized Bubble Model

The comparison of cosmological and microscopic measurements in eqs. (2.65) and (2.66), is precise, but it is not accurate: it is based on a highly idealized model system and is not expected to produce exact agreement with the physical cosmological constant. In the real QCD vacuum, coherent gluonic wave states have a more complex 4D structure than the bubble model. The quantum wave function of virtual gluonic matter is not a homogeneous sphere, that of quarks is not a thin shell, actual pion states are not radially homogeneous, and virtual stress is not isotropic as in the bubble. A more stringlike gluon state, which has less repulsive gravity, would require a smaller value of R_0 to match the observed cosmic acceleration. The estimate just given also does not allow for finite quark mass, $m \neq 0$, but since physical quark masses have $m << m_\pi$, this difference produces only a small fractional change, as shown in the solution above (eq. (2.52)).

There are also ambiguities in our idealized application of the correspondence principle to virtual orbits, which depend on how quantum gravity actually works in detail. For example, the volume average taken above (eq. (2.58)) uses the mean acceleration of bodies relative to the center of the bubble over an orbit, but it might be more accurate to include a directional projection of the component of radial acceleration onto the opposite hemisphere of the causal diamond. Such a projection factor would change the answer by a small numerical factor. In principle, nonlocally-coherent gravitational effects of vacuum QCD fluctuations could be better approximated with an explicit calculation of nonlinear quantum field dynamics.

2.4.4 Remarks

Why QCD?

It is natural to ask, why QCD? What's special about its vacuum, compared to the other fields, that make it source the cosmological constant?

In a coherent relational model of locality, there are straightforward physical reasons why the gravitational effect of vacuum fluctuations for most standard model fields should vanish. The classical gravity of a null particle with momentum p is simple: it creates a null shock with a displacement $\delta\tau = Gp/c^4$, with an observable portion that depends on the location of the particle relative to observer [Mackewicz and Hogan, 2022]. A zero-point field vacuum excitation, generated by a creation operator on an infinite plane wave mode, creates a completely delocalized state, so according to the correspondence principle, there is no observable gravitational effect: essentially, everything "moves together".

This argument applies to the Standard Model fields whose interactions and correlations fall off in the infrared. As noted above, the vacuum fluctuations of gluons are uniquely different from those of other forces. The "IR slavery" of the QCD vacuum confines baryons into bags, and leads to a finite range at the Fermi scale for strong Yukawa interactions mediated by pions. The same effect makes QCD vacuum gravity different from that of the other forces: the vacuum fluctuations of QCD correspond to coherent localized bubbles of energy flow on the Fermi scale, so the argument just given for delocalized vacuum states does not apply. Renormalization required for quantum field theory fails to account correctly for gravitational entanglement of causal structure with long wavelength modes [Hollands and Wald, 2004, Stamp, 2015], so it is plausible that the IR slavery of vacuum QCD fluctuations leads to different gravitational effects from other fields.

Outside of hadrons, the QCD vacuum at low temperature is a coherent condensate, whose mean gravitating density is negligible [Brodsky and Shrock, 2011]. Its fluctuations resemble the lightest resonant excitations, pions, which are spatially extended but localized. Nearly all of their virtual energy comes from the massless gluon field. In the gluonic bubble model, fluctuations in the tensile gluon interaction energy produce a small but cosmologically detectable repulsive gravity. Estimates of the effective equation of state from field theory [Schutzhold, 2002, Bjorken, 2003, 2010, Klinkhamer and Volovik, 2009, Poplawski, 1990]

reproduce the estimate from our bubble model.

The other non-abelian forces of the Standard Model, the weak interactions, are mediated by massive particles with a short range, and the nonlocal space-time correlations of their vacuum fluctuations are qualitatively different from QCD. For these, the "zero momentum mode" of fluctuations takes the form of a globally spatially uniform scalar condensate with homogeneous fluctuations around the minimum of an effective potential. This Higgs condensate, whose order parameter describes the low-temperature vacuum expectation value of the effective potential, apparently has zero gravitation [Weinberg, 1989]. As explained in the Appendix, the difference in gravitational effect from the space-filling QCD vacuum can be understood from an exponential suppression of the trace anomaly at weaker coupling strength [Schutzhold, 2002].

Causal Coherence of Virtual Fluctuations

The bubble model illustrates classically how a fluctuation could have a durable macroscopic physical effect if positional relationships among world lines are determined by coherent causal diamonds. In such an emergent relational holographic picture, classical locality emerges as a consistent approximation on large scales, based on relationships of a causal diamond with those it is nested in. Exact relational positions within causal diamonds are indeterminate.

In our model, systematic secular effects of fluctuations are assumed to lead to a durable effect on the classical metric. This hypothesis leads to the assumption used in our estimate of mean acceleration of test particles, relative to the center of the bubble. On average, the acceleration applies to test particles in relation to the future light cones on the opposite side of a pion-like causal diamond vacuum fluctuation. The coherence propagates local coherent acceleration to the future light cone of a microscopic causal diamond, which leads to coherent acceleration of the same magnitude on a cosmic scale.

The bubble model illustrates concretely how causal coherence of virtual fluctuation states

is connected with the small nonzero value of the cosmological constant. According to this scenario, the wildly wrong estimate of vacuum fluctuation density in eq. (2.1) results from an incorrect physical interpretation of vacuum energy that does not take directional causal coherence of virtual states into account; it arises from the incorrect model of locality built into a particular interpretation of field theory.

Careful studies of entanglement and decoherence in virtual field fluctuations confirm the need to account for causal consistency to avoid apparent paradoxes with nonrelativistic quantum thought-experiments [Danielson et al., 2022, Belenchia et al., 2019]. The decomposition into modes that are used to construct a vacuum state— the differentiation between radiation and vacuum— depends on the choice of Cauchy surfaces used to describe the system. Apparent paradoxes are resolved when field states are measured on Cauchy surfaces that correspond to correlated measurements.

Similar causal coherence of primordial virtual fluctuations has recently been used in a model that explains some observed anomalies of cosmological anisotropy at large angular separation [Hogan and Meyer, 2022, Hogan et al., 2023]. In that context, directional hemispherical coherence leads to a causal "shadow" in primordial virtual correlation, which is observed as a symmetry of temperature correlations at large angles.

Why Now?

Typically, field-based models of cosmic acceleration require introduction of new fields with new, arbitrary and very small dimensionless parameters, in some cases accompanied by an anthropic explanation [Weinberg, 1989]. In the gluonic-bubble scenario, Λ is not an independent parameter, but should have a precisely calculable value from Standard Model field fluctuations and standard semiclassical gravity.

In principle, this scenario roughly accounts for the well-known puzzle sometimes nicknamed the "why now" coincidence— the fact that the timescale associated with fundamental

cosmic acceleration coincides with the current age of the universe, which in turn presumably is determined by astrophysical timescales, such as those determined by stellar evolution. The very long evolution timescale of stars and other astrophysical systems in Planck units originates mainly from the cube of the nucleon mass [Hogan, 2000]:

$$T_{astro}/t_P \sim (m_P/m_{proton})^3. \tag{2.67}$$

(Additional dimensionless factors that are numerically less significant, such as the electromagnetic coupling and electron/nucleon mass ratio, depend on the specific astrophysical system.) The exponentially large dimensionless number m_P/m_{proton}, which expresses the weakness of gravity on a nuclear scale, appeared mysterious to Planck, Eddington and Dirac, but now has a natural interpretation in the context of modern unified field theory, because of the logarithmic running of the QCD coupling constant with energy scale [Wilczek, 1999]. In any case, because nucleon masses are determined by the same scale that fixes masses of pions and QCD vacuum fluctuation bubbles, the astrophysical timescale T_{astro} naturally (roughly) coincides with the bubble model for T_Λ, since they originate from the same large dimensionless number.

2.5 Gravity of a Gluonic String Model

2.5.1 Non-rotating string model

We now consider the gravitational effect if the gluonic material does not uniformly fill a causal diamond as it does in the bubble model. Consider an extended particle of total mass M represented by two "quarks" of mass $m << M$ connected by a one dimensional string with mass per length $\mu = \mu_0 M^2(c/\hbar)$, where μ_0 is a dimensionless parameter that characterizes the gluonic tension. The system has zero angular momentum, so the quarks travel on radial trajectories connected by the straight string. It starts with zero length, stretches to length

$L_M = \hbar/\mu_0 Mc$, then re-contracts under the string tension.

For a classical model of strongly interacting gluonic quantum field excitations like pions, we can take the parameter μ_0 to be less than but of the order unity. Values $\mu_0 << 1$ correspond to longer strings, which break apart into many shorter strings as new quark pairs are created. Values $\mu_0 > 1$ describe systems smaller than the de Broglie wavelength, so they do not correspond to physical quantum states.

As in the bubble model, very light quarks of mass $m << M$, with a negligible fraction of the total mass, start with very high gamma-factor $\gamma = M/2m$ relative to the center, so the trajectories are nearly null. Their kinetic energy is converted to string energy as they travel. Eventually $\gamma \approx 1$, and for a time short compared to L_M/c, they enter a subrelativistic regime where the string tension turns them around. For pion-like systems with $m << M$, the short subrelativistic regime is a small fraction of the whole trajectory, so the main effects do not depend strongly on the value of m.

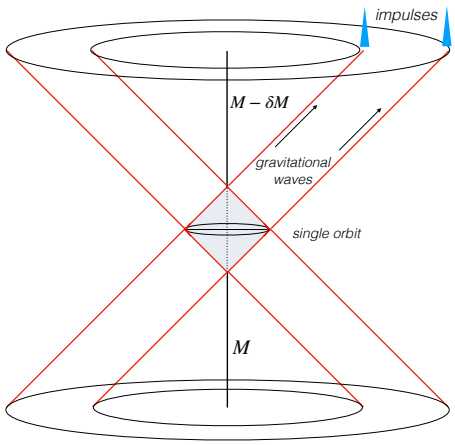

Figure 2.5: Causal diagram of gravitational radiation from a single gluonic string orbit. For $M >> m$, displacement is concentrated near anisotropic, spherical null shocks.

2.5.2 Gravitational Waves

As shown in more detail in the linear solution below, a gluonic string produces gravitational waves (fig. 2.5). A simple estimate of the radiation rate from dimensional arguments shows

how the rate of energy loss scales with M. In one orbit, a fully relativistic string with deficit angle $\delta\theta$ radiates a fraction

$$\delta\theta \sim \delta M/M \sim \mu G/c^2 \sim \mu\hbar/cm_P^2 \tag{2.68}$$

of its energy as gravitational radiation. For a gluonic string of length $L_M = \hbar/\mu_0 Mc$ with $m << M$, the decay rate by gravitational radiation in Planck units is about

$$t_P/\tau_d \sim \mu_0^2(M/m_p)^3. \tag{2.69}$$

The string model displays roughly the same energy flow between QCD fluctuations and the gravitational vacuum as the bubble model, but it does not produce the same mean classical repulsion as gravity from bubble-like fluctuations.

2.5.3 Linear String Solution for $m \geq 0$

i. Equations of Motion

For all computations in this section we will work in units where $c = 1, G = 1$ and restore units when needed. The energy-momentum tensor

$$T^{ab} = T_s^{ab} + T_p^{ab} \tag{2.70}$$

consists of two parts: that of particles (representing quarks),

$$T_p^{ab} = m\delta(x)\delta(y)(\delta(z - z_1(t))v_1^a u_1^b + 1 \leftrightarrow 2), \tag{2.71}$$

whose four-velocity is

$$u_a = \gamma v_a = \gamma_{1,2}(1, 0, 0, \dot{z}_{1,2}), \tag{2.72}$$

and that of a string (representing gluons),

$$T_s^{ab} = \mu\delta(x)\delta(y)\mathcal{T}^{ab}\theta(z - z_2(t))\theta(z_1(t) - z), \tag{2.73}$$

where μ is the constant mass per unit length of the string, $\mathcal{T}^{ab} \equiv t^a t^b - z^a z^b$, and $\theta(x)$ is the heaviside step function which is 1 for $x > 0$ and vanishes elsewhere.

The equations of motion are similar for the two models, the string and the bubble. They are not identical: in the bubble, the quark surface mass density decreases with radius, so the inward acceleration at the edge for constant p increases with radius.The difference between solutions is small for $m << M$, since the turnaround happens within a small fractional change in radius.

In the string model, conservation of total stress-energy $\nabla_a T^{ab} = 0$ gives an equation of motion for the positions of the quarks $z_{1,2}(t)$,

$$\frac{d}{dt}(\gamma_{1,2}\dot{z}_{1,2}) = \mp\frac{\mu}{m} \equiv \mp\alpha. \tag{2.74}$$

The solution for a uniformly accelerated relativistic particle with constant (proper) acceleration α, initial 3-velocity v_0, and initial position $z_0 = 0$ is given by

$$z_{1,2}(t) = \pm\frac{1}{\alpha}[\gamma_0 - (1 + (\gamma_0 v_0 - \alpha t)^2)^{1/2}]. \tag{2.75}$$

The acceleration parameter is given by $\alpha = \mu/m$. Note that the turnaround time (or equivalently, the duration of time for which the particle is non-relativistic) is approximately $\delta t \sim 1/\alpha \sim L/\gamma_0$.

In the string model, we will see later that the peaks in the "radiative" part of the curvature occur at the retarded time associated with the turnaround of each particle. The period of the trajectory is $T = 2\gamma_0 v_0/\alpha$. Therefore the fraction of time during which the trajectory is non-

ultra-relativistic is $\delta t/T \sim 1/\gamma_0 v_0 \sim 1/\gamma_0 << 1$. However, we will see later that the relative acceleration experienced by nearby test bodies scales like $\dot{v} \sim \alpha^2$, so that $\delta v \sim \dot{v}\delta t \sim \alpha$.

ii. Gravitational Effect

To determine the gravitational effect of such a system, we begin with the linearized Einstein equations (eq. (14)) in the Lorenz gauge $\nabla^a \bar{h}_{ab} = 0$. The solution to this equation is found by integrating over the intersection of the source world sheet with the past light cone, as in eq. (15). Since the delta function depends both explicitly on $\vec{x}'$ and implicitly through $t_{\rm ret}$, we need to use the Jacobian of the coordinate transformation to evaluate the integrals of the delta functions.

The metric perturbation associated with the low mass particles is

$$\bar{h}^p_{ab} = \frac{4m\gamma_1 v^1_a v^1_b}{\alpha_1 |\vec{x} - \vec{X}_1(t_{\rm ret})|} + \frac{4m\gamma_2 v^2_a v^2_b}{\alpha_2 |\vec{x} - \vec{X}_2(t_{\rm ret})|} \tag{2.76}$$

where

$$\alpha_{1,2} = 1 - \hat{n}_{1,2} \cdot \frac{d\vec{X}_{1,2}}{dt}(t_{\rm ret}) \tag{2.77}$$

$$\hat{n}_{1,2} = \frac{\vec{x} - \vec{X}_{1,2}(t_{\rm ret})}{|\vec{x} - \vec{X}_{1,2}(t_{\rm ret})|} \tag{2.78}$$

From this point forward, evaluation at retarded time will be understood unless explicitly stated otherwise. The metric perturbation associated with the string is

$$\bar{h}^s_{ab} = 4\mu \ln \left(\frac{z - z_2 + \sqrt{s^2 + (z - z_2)^2}}{z - z_1 + \sqrt{s^2 + (z - z_1)^2}} \right) \mathcal{T}_{ab} \tag{2.79}$$

where $s^2 = x^2 + y^2$ denotes the transverse distance from the string. We note here that while in the case of the infinite string the spacetime is flat with an angular deficit, the dynamic string does in fact produce curvature. We are most interested in the leading order in $1/r$

behavior of the metric perturbation. In this limit, $\hat{n} \to \hat{x}$ and $t_{\rm ret} \approx t - r + \cos\theta z_{1,2}(t_{\rm ret})$.

$$\bar{h}^s_{ab} = \frac{4\mu}{r}(z_1 - z_2)\mathcal{T}_{ab} + \mathcal{O}\left(\frac{1}{r^2}\right) \tag{2.80}$$

$$\bar{h}^p_{ab} = \frac{4m}{r}\left(\frac{\gamma_1 v^1_a v^1_b}{1 - \cos\theta \dot{z}_1(t_{\rm ret})} + 1 \leftrightarrow 2\right) + \mathcal{O}\left(\frac{1}{r^2}\right) \tag{2.81}$$

In the far field limit, the retarded time can be solved explicitly as a function of $u = t - r$ and θ.

$$t^{1,2}_{\rm ret} = \frac{1}{\alpha \sin^2\theta}\left(u\alpha \pm \gamma_0 \cos\theta \mp |\cos\theta| \sqrt{(\sin^2\theta + (u\alpha \pm \gamma_0 \cos\theta)^2)}\right) \tag{2.82}$$

Since we are primarily interested in the far field behavior of the curvature, we need only consider derivatives which act on the time dependent terms in eq. (2.80) and (2.81). One can show that $\partial t_{\rm ret}/\partial t = 1/\alpha_{1,2}$ and $\nabla t_{\rm ret} = -\hat{n}/\alpha_{1,2}$. In other words, $\nabla_a f(t_{\rm ret}) = -K_a \dot{f}(t_{\rm ret})/\alpha_{1,2}$, where $K_a = -\nabla_a u = t_a + r_a$ is a radially out-going null vector. In this limit, the linearized Riemann tensor simplifies to

$$R_{abcd} \approx 2K_{[a}K_{|[d}\ddot{\bar{h}}_{c]|b]} \tag{2.83}$$

The relevant components of the Riemann tensor for eq. (9) are plotted in Fig. fig. 2.6 as a function of the retarded time coordinate $u = t - r$. Note the sharp spikes in curvature, which occur at the turnaround points of the quarks as viewed by a stationary observer.

The effective stress-energy tensor for the gravitational waves is given by

$$T^{\rm GW}_{ab} = \frac{1}{32\pi}\left\langle \bar{h}_{cd,a}\,\bar{h}^{cd}{}_{,b} - \frac{1}{2}\bar{h}_{,a}\,\bar{h}_{,b} - \bar{h}^{cd}{}_{,d}\,\bar{h}_{cb,a} - \bar{h}^{cd}{}_{,d}\,\bar{h}_{ca,b} \right\rangle \tag{2.84}$$

where $\langle ... \rangle$ denotes an average over several wavelengths of the radiation. Although this object is not gauge invariant (and therefore its physical interpretation is unclear), the total

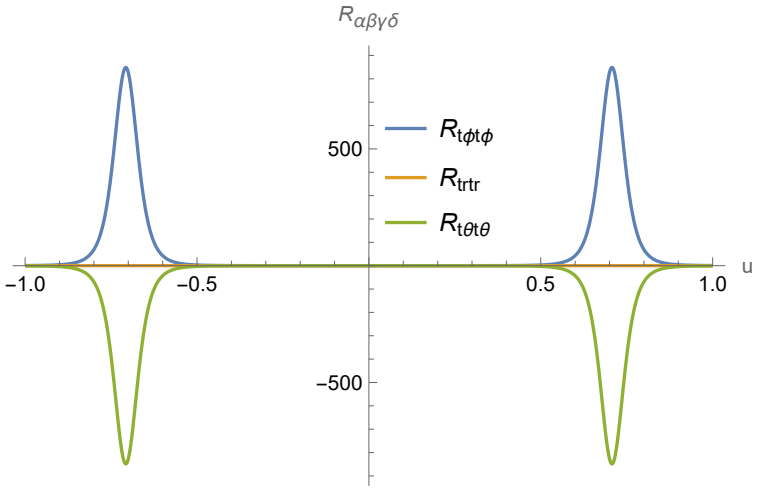

Figure 2.6: Components of the Riemann curvature tensor from eq. (9) plotted as a function of retarded time $u = t - r$ for $\gamma_0 = 10, \alpha = 10, \theta = \pi/4$. The curvature spikes at the retarded times associated with the turnaround of each quark. Due to the highly relativistic motion, the turnaround is no longer simultaneous as seen by an observer away from the equator ($\theta = \pi/2$).

integrated flux of energy to null infinity as defined by

$$P = -\lim_{r\to\infty} \int T_{0a} dS^a \tag{2.85}$$

is gauge invariant and is therefore a physically meaningful quantity. It turns out that the dynamics of the string do not contribute directly to the stress energy of the gravitational waves in this setup, although the string does indirectly contribute by determining the dynamics of the quarks. Restoring units, the total integrated power in the string model scales like

$$P = f(\gamma_0)\alpha^2 m^2 G c^{-1} \tag{2.86}$$

where $f(\gamma_0)$ is plotted in fig. 2.7 on a log-linear scale. We see that the asymptotic scaling of P is logarithmic in γ_0, hence confirming the previous assumption that the power does not strongly depend on the mass of the quarks in the $m << M$ limit. For a pion mass of 135 MeV and quark masses of about $3 - 5$ MeV, we get $\gamma_0 = M/2m \sim 10^1$ and $f(\gamma_0) \sim 10^1$. In

agreement with the estimate given by eq. (2.69), the timescale of decay is

$$\tau_d^{-1} = \frac{P}{M} \sim 10^1 \mu_0^2 (M/m_p)^3 \tau_p^{-1} \tag{2.87}$$

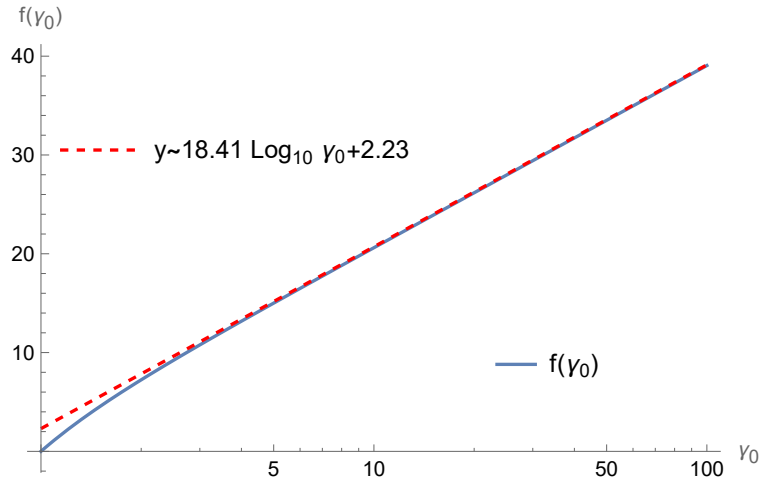

Figure 2.7: Plot of $f(\gamma_0)$ in eq. (2.86) on a log-linear scale, demonstrating an asymptotically logarithmic scaling of the power.

2.6 Strong Energy Condition, Quantum Trace Anomaly, and Dimensional Dependence

We now explore how the particular nature of the QCD interactions can allow for a repulsive gravitational effect. Consider a congruence of timelike geodesics described by a vector field u_a. The expansion, shear, and twist of the congruence are defined by

$$\theta = q_{ab} \nabla^a u^b \tag{2.88}$$

$$\sigma_{ab} = q_a^c q_b^d \nabla_{(c} u_{d)} - \frac{1}{3} \theta q_{ab} \tag{2.89}$$

$$\omega_{ab} = q_a^c q_b^d \nabla_{[c} u_{d]} \tag{2.90}$$

where q_{ab} denotes the spatial part of the metric that is orthogonal to u_a, and $(a,b), [a,b]$ denote symmetrization and antisymmetrization of indices, respectively. Raychaudhuri's equation tells us how the expansion evolves with time.

$$\frac{d\theta}{d\tau} = -\frac{1}{3}\theta^2 - \sigma_{ab}\sigma^{ab} + \omega_{ab}\omega^{ab} - R_{ab}u^a u_b \tag{2.91}$$

Here R_{ab} denotes the Ricci tensor. As is typically done, we will ignore the twist. For a congruence which initially has zero expansion and shear, we have (after using the Einstein field equations to replace R_{ab} with T_{ab})

$$\left.\frac{d\theta}{d\tau}\right|_{t=0} = -8\pi\left(T_{ab} - \frac{1}{2}g_{ab}T\right)u^a u^b \tag{2.92}$$

where $T = g^{ab}T_{ab}$, which evaluates to $T = -T_{00} + T_{11} + T_{22} + T_{33}$ in global inertial coordinates. For a perfect fluid in 3 spatial dimensions (in units where $c = 1$),

$$T_{ab} = \mathrm{diag}(\rho, p, p, p), \tag{2.93}$$

so eq. (2.92) becomes

$$\left.\frac{d\theta}{d\tau}\right|_{t=0} = -4\pi(\rho + 3p) \tag{2.94}$$

Therefore if the perfect fluid obeys an equation of state $p < -\rho/3$ (such that the strong energy condition $R_{ab}u^a u^b > 0$ is violated), the expansion of the congruence will initially be positive, leading to a repulsive gravitational effect. As the expansion and shear grow, the RHS of eq. (2.91) will eventually reach zero, but the sign of the rate of change of expansion can never become negative.

Now consider another fundamental constraint: a perfect fluid composed purely of a classical non-abelian gauge field (e.g., massless noninteracting point particles, such as photons), the equation of state is $p = \rho/3$, which does not violate the strong energy condition. The

form of the field strength tensor in classical Yang Mills theory is such that the trace of the stress-energy tensor always vanishes, similar to classical Maxwell theory. However, quantum interactions between the gluons and quarks and the self-interaction of gluons lead to what is known as a trace anomaly, i.e. a non-vanishing of the trace of the quantum stress energy tensor.

In order for the strong energy condition to be violated by quantum interactions, eq. (2.88) tells us that the equation of state must satisfy $\rho + T/2 < 0$, or $T < -2\rho$. For a perfect fluid, we have $T = -\rho + 3p$. This puts a constraint on the magnitude of the trace anomaly if QCD vacuum fluctuations are to serve as the source of accelerating cosmic expansion. It has been hypothesized Schutzhold [2002] that this trace anomaly can produce the violation of the strong energy condition needed to produce a repulsive gravitational effect.

The vanishing of the trace of the stress-energy tensor is synonymous with conformal invariance of the action of a field theory, i.e. $S = \int d^4x\sqrt{-g}\mathcal{L}$ is invariant under $g_{\mu\nu} \rightarrow \Omega(x^\alpha)g_{\mu\nu}$. In ref. Schutzhold [2002] it is shown that this conformal invariance is preserved under the standard QFT renormalization procedures for *free* fields in flat space but *not* for self-interacting fields in flat space or free fields in curved spacetimes. It is estimated there that the self-interacting gluonic field gives rise to a negative energy density and pressure proportional to the renormalization group β function, with a corresponding cosmological constant that is many orders of magnitude too large.

According to our interpretation, where the gravitational effect of virtual fluctuations is evaluated using a causally coherent bubble model, the magnitude is about right. This result is consistent with the idea that active gravity entangles long wavelength field modes with causal structure, which is not accounted for in standard renormalization proceduresHollands and Wald [2004], Stamp [2015].

Although the sharp boundary and spherical symmetry of the bubble model are artificial, we conjecture that the physical gravitational effect is indeed microscopic, localized at the

Fermi scale. Unlike the model sketched in ref. Schutzhold [2002], the cosmic acceleration is a true cosmological constant, with a value determined entirely by the properties of the stable QCD ground state vacuum. These arguments suggest that at very high temperatures in the early universe, when QCD had significantly weaker interactions, the value was much smaller, but there are no observable consequences of this variation.

Schutzhold [2002] also shows that free fields in curved space gives a positive energy density with a cosmological constant that is many orders of magnitude too small, which supports our conjecture that fluctuations of the other Standard Model fields do not contribute significantly to the gravitational energy of the vacuum. The effects of the anomaly are nonperturbative, and are exponentially suppressed for coupling constants that are not of order unity.

Finally, we address why the bubble model of the pion behaves differently from the string model for producing a repulsive gravity. Although the string model of the pion is commonly used as a toy model in other contexts, it does not work as a gravitational model because of the dimensionality of the matter distribution. In order to violate the strong energy condition in D spatial dimensions, the fluid must satisfy

$$T_{00} + \frac{1}{2}T = \rho + \frac{1}{2}(-\rho + Dp) < 0 \rightarrow \rho + Dp < 0 \tag{2.95}$$

Therefore, a pressure $p = -\rho$ in $D = 1$ spatial dimensions (i.e. a straight string) cannot violate the strong energy condition: more than one dimension of tension is needed to account for cosmic acceleration.

2.7 Conclusion

The gluonic bubble model demonstrates the classical gravitational coupling of a single pion-like oscillation with geometry. Our proposal for the cosmological constant is that fluctuations in the QCD vacuum have a similar relationship with gravity. Delocalized zero-point fluc-

tuations of field vacua contribute nothing to the mean density that couples to gravity, but locally coherent fluctuations have a net repulsive effect that mimics a uniform cosmological constant. This effect occurs for the strong interactions in particular because of gluonic tension, represented in our toy model by highly tensile gluonic gas. Our model shows how this works geometrically in classical systems, and why a nonlocally coherent 4D structure is needed to obtain a net repulsive gravitational effect.

Although the bubble model adopted here is a simplified idealization of real QCD vacuum states, the essential elements that create the cosmological constant of the magnitude estimated here— nonlocal directional causal coherence of vacuum states, and a tension from the strong non-abelian self-interactions of gluon fields— must also appear in the states of the physical QCD vacuum. In this scenario, the absolute value of the physical cosmological constant can in principle be calculated exactly from a nonlinear computation of spacelike correlations of 4D mass-energy flows in the virtual QCD vacuum. Such a calculation would allow more precise tests than the approximate agreement obtained here with a highly idealized picture.

REFERENCES

E. G. Adelberger, J. H. Gundlach, B. R. Heckel, S. Hoedl, and S. Schlamminger. Torsion balance experiments: A low-energy frontier of particle physics. *Progress in Particle and Nuclear Physics*, 62(1):102–134, January 2009. doi:10.1016/j.ppnp.2008.08.002.

P. C. Aichelburg and R. U. Sexl. On the gravitational field of a massless particle. *General Relativity and Gravitation*, 2(4):303–312, Dec 1971. ISSN 1572-9532. doi:10.1007/BF00758149. URL https://doi.org/10.1007/BF00758149.

Ahmed Almheiri, Thomas Hartman, Juan Maldacena, Edgar Shaghoulian, and Amirhossein Tajdini. The entropy of Hawking radiation. 6 2020.

B. Andersson, G. Gustafson, G. Ingelman, and T. Sjöstrand. Parton fragmentation and string dynamics. *Physics Reports*, 97(2):31–145, 1983. ISSN 0370-1573. doi:https://doi.org/10.1016/0370-1573(83)90080-7. URL https://www.sciencedirect.com/science/article/pii/0370157383900807.

Thomas Banks and Kathryn M. Zurek. Conformal Description of Near-Horizon Vacuum States. 8 2021.

Tom Banks. Holographic Space-time and Quantum Information. *Front. in Phys.*, 8:111, 2020. doi:10.3389/fphy.2020.00111.

Tom Banks and Patrick Draper. Remarks on the Cohen-Kaplan-Nelson bound. *Phys. Rev. D*, 101:126010, Jun 2020. doi:10.1103/PhysRevD.101.126010. URL https://link.aps.org/doi/10.1103/PhysRevD.101.126010.

C Barrabes. Singular hypersurfaces in general relativity: a unified description. *Classical and Quantum Gravity*, 6(5):581, may 1989. doi:10.1088/0264-9381/6/5/003. URL https://dx.doi.org/10.1088/0264-9381/6/5/003.

C. Barrabès and P. A. Hogan. Colliding impulsive gravitational waves and a cosmological constant. *Phys. Rev. D*, 92:044032, Aug 2015. doi:10.1103/PhysRevD.92.044032. URL https://link.aps.org/doi/10.1103/PhysRevD.92.044032.

C. Barrabès and W. Israel. Thin shells in general relativity and cosmology: The lightlike limit. *Phys. Rev. D*, 43:1129–1142, Feb 1991. doi:10.1103/PhysRevD.43.1129. URL https://link.aps.org/doi/10.1103/PhysRevD.43.1129.

C. Barrabès and P. A. Hogan. Collisions of Shock Waves in General Relativity. *Progress of Theoretical Physics*, 126(6):1157–1165, 12 2011. ISSN 0033-068X. doi:10.1143/PTP.126.1157. URL https://doi.org/10.1143/PTP.126.1157.

Daniel Baumann. Inflation. In *Physics of the large and the small, TASI 09*, pages 523–686, 2011. doi:10.1142/9789814327183_0010. URL https://inspirehep.net/record/827549/files/arXiv:0907.5424.pdf.

Alessio Belenchia, Robert M. Wald, Flaminia Giacomini, Esteban Castro-Ruiz, Časlav Brukner, and Markus Aspelmeyer. Information Content of the Gravitational Field of a Quantum Superposition. *Int. J. Mod. Phys. D*, 28(14):1943001, 2019. doi:10.1142/S0218271819430016.

J. D. Bjorken. Emergent Photons and Gravitons:The Problem of Vacuum Structure. In *Proceedings, 5th Meeting on CPT and Lorentz Symmetry (CPT 10)*, pages 1–5, 2010. doi:10.1142/9789814327688_0001. URL `http://inspirehep.net/record/864127/files/arXiv:1008.0033.pdf`.

James D. Bjorken. Cosmology and the standard model. *Phys. Rev.*, D67:043508, 2003. doi:10.1103/PhysRevD.67.043508.

H. Bondi. Plane gravitational waves in general relativity. *Nature*, 179, 1957. doi:https://doi.org/10.1038/1791072a0.

H. Bondi, M. van der Burg, and A. Metzner. Gravitational waves in general relativity, vii. waves from axi-symmetric isolated system. *Proc. Roy. Soc. Lond. A.*, 269, 1962. URL `https://doi.org/10.1098/rspa.1962.0161`.

Stanley J. Brodsky and Robert Shrock. Condensates in quantum chromodynamics and the cosmological constant. *Proceedings of the National Academy of Sciences*, 108(1):45–50, 2011. doi:10.1073/pnas.1010113107. URL `https://www.pnas.org/doi/abs/10.1073/pnas.1010113107`.

C. M. Caves. Quantum-mechanical radiation-pressure fluctuations in an interferometer. *Phys. Rev. Lett.*, 45:75, 1980a.

C. M. Caves. Quantum-mechanical noise in an interferometer. *Phys. Rev.*, D23:1693, 1980b.

A. Chou, H. Glass, H. R. Gustafson, C. J. Hogan, B. L. Kamai, O. Kwon, R. Lanza, L. McCuller, S. S. Meyer, J. Richardson, C. Stoughton, R. Tomlin, and R. Weiss. Interferometric Constraints on Quantum Geometrical Shear Noise Correlations. *Class. Quant. Grav.*, 34 (16):165005, 2017. doi:10.1088/1361-6382/aa7bd3.

C J S Clarke and T Dray. Junction conditions for null hypersurfaces. *Classical and Quantum Gravity*, 4(2):265, mar 1987. doi:10.1088/0264-9381/4/2/010. URL `https://dx.doi.org/10.1088/0264-9381/4/2/010`.

A. G. Cohen, D. B. Kaplan, and A. E. Nelson. Effective field theory, black holes, and the cosmological constant. *Phys. Rev. Lett.*, 82:4971, 1999.

Andrew G. Cohen and David B. Kaplan. Gravitational contributions to the electron g-factor. *arXiv e-prints*, art. arXiv:2103.04509, March 2021.

Daine L. Danielson, Gautam Satishchandran, and Robert M. Wald. Gravitationally mediated entanglement: Newtonian field versus gravitons. *Phys. Rev. D*, 105:086001, Apr 2022.

doi:10.1103/PhysRevD.105.086001. URL https://link.aps.org/doi/10.1103/PhysRevD.105.086001.

Tevian Dray and Gerard 't Hooft. The gravitational shock wave of a massless particle. *Nuclear Physics B*, 253:173 – 188, 1985. ISSN 0550-3213. doi:https://doi.org/10.1016/0550-3213(85)90525-5. URL http://www.sciencedirect.com/science/article/pii/0550321385905255.

J. Ehlers and W. Kundt. *Gravitation: an Introduction to Current Research*. 1962.

David Garfinkle. Metrics with distributional curvature. *Classical and Quantum Gravity*, 16 (12):4101, dec 1999. doi:10.1088/0264-9381/16/12/324. URL https://dx.doi.org/10.1088/0264-9381/16/12/324.

G. Gemelli. Gravitational waves and discontinuous motions. *Gen. Relativ. Gravit.*, 29: 161–178, 1997. doi:10.1023/A:1010283826916. URL https://doi.org/10.1023/A:1010283826916.

Robert Geroch and Jennie Traschen. Strings and other distributional sources in general relativity. *Phys. Rev. D*, 36:1017–1031, Aug 1987. doi:10.1103/PhysRevD.36.1017. URL https://link.aps.org/doi/10.1103/PhysRevD.36.1017.

Steven B. Giddings. Nonviolent unitarization: basic postulates to soft quantum structure of black holes. *Journal of High Energy Physics*, 2017(12), Dec 2017. ISSN 1029-8479. doi:10.1007/jhep12(2017)047. URL http://dx.doi.org/10.1007/JHEP12(2017)047.

Steven B. Giddings. Black holes in the quantum universe. *Phil. Trans. Roy. Soc. Lond.*, A377(2161):20190029, 2019. doi:10.1098/rsta.2019.0029.

Ray Hagimoto, Craig Hogan, Collin Lewin, and Stephan S. Meyer. Symmetries of CMB temperature correlation at large angular separations. *The Astrophysical Journal*, 888(2): L29, jan 2020. doi:10.3847/2041-8213/ab62a0. URL https://doi.org/10.3847%2F2041-8213%2Fab62a0.

Craig Hogan. Nonlocal entanglement and directional correlations of primordial perturbations on the inflationary horizon. *Phys. Rev. D*, 99:063531, Mar 2019. doi:10.1103/PhysRevD.99.063531. URL https://link.aps.org/doi/10.1103/PhysRevD.99.063531.

Craig Hogan. Cosmological Constant in Coherent Quantum Gravity. *Int. J. Mod. Phys. D*, 29(14):2042004, 2020a. doi:10.1142/S0218271820420043.

Craig Hogan. Pattern of perturbations from a coherent quantum inflationary horizon. *Classical and Quantum Gravity*, 37(9):095005, apr 2020b. doi:10.1088/1361-6382/ab7964. URL https://doi.org/10.1088%2F1361-6382%2Fab7964.

Craig Hogan and Stephan S. Meyer. Angular correlations of causally-coherent primordial quantum perturbations. 2021.

Craig Hogan and Stephan S Meyer. Angular correlations of causally-coherent primordial quantum perturbations. *Classical and Quantum Gravity*, 39(5):055004, feb 2022. doi:10.1088/1361-6382/ac4829. URL https://doi.org/10.1088/1361-6382/ac4829.

Craig Hogan, Stephan S. Meyer, Nathaniel Selub, and Frederick Wehlen. Angular correlations on causally-coherent inflationary horizons. 3 2023.

Craig J. Hogan. Why the universe is just so. *Rev. Mod. Phys.*, 72:1149–1161, 2000. doi:10.1103/RevModPhys.72.1149.

Stefan Hollands and Robert M. Wald. Essay: Quantum field theory is not merely quantum mechanics applied to low energy effective degrees of freedom. *General Relativity and Gravitation*, 36:2595–2603, Dec 2004. ISSN 0001-7701.

Stefan Hollands, Akihiro Ishibashi, and Robert M Wald. BMS supertranslations and memory in four and higher dimensions. *Classical and Quantum Gravity*, 34, 2016. URL https://iopscience.iop.org/article/10.1088/1361-6382/aa777a.

W. Israel. Singular hypersurfaces and thin shells in general relativity. *Il Nuovo Cimento B*, 44:1–14, 1966. doi:10.1007/BF02710419. URL https://doi.org/10.1007/BF02710419.

D. J. Kapner, T. S. Cook, E. G. Adelberger, J. H. Gundlach, B. R. Heckel, C. D. Hoyle, and H. E. Swanson. Tests of the Gravitational Inverse-Square Law below the Dark-Energy Length Scale. *Prl*, 98(2):021101, January 2007. doi:10.1103/PhysRevLett.98.021101.

F. R. Klinkhamer and G. E. Volovik. Gluonic vacuum, q-theory, and the cosmological constant. *Phys. Rev. D*, 79:063527, Mar 2009. doi:10.1103/PhysRevD.79.063527. URL https://link.aps.org/doi/10.1103/PhysRevD.79.063527.

Kris Mackewicz and Craig Hogan. Gravity of two photon decay and its quantum coherence. *Classical and Quantum Gravity*, 39(7):075015, mar 2022. doi:10.1088/1361-6382/ac5377. URL https://dx.doi.org/10.1088/1361-6382/ac5377.

T. Padmanabhan. Cosmological constant: The Weight of the vacuum. *Phys. Rept.*, 380: 235–320, 2003. doi:10.1016/S0370-1573(03)00120-0.

Igor Pikovski, Magdalena Zych, Fabio Costa, and Časlav Brukner. Time Dilation in Quantum Systems and Decoherence. *New Journal of Physics*, 19(2):025011, feb 2017. doi:10.1088/1367-2630/aa5d92. URL https://doi.org/10.1088%2F1367-2630%2Faa5d92.

Eric Poisson. A reformulation of the barrabes-israel null-shell formalism, 2002.

Nikodem J. Poplawski. Cosmological constant from quarks and torsion. *Annalen Phys.*, 523: 291–295, 1990. doi:10.1103/PhysRevD.43.1129.

J. Prat, C. Hogan, C. Chang, and J. Frieman. Vacuum energy density measured from cosmological data. *JCAP*, 06(06):015, 2022. doi:10.1088/1475-7516/2022/06/015.

A. Rätzel, M. Wilkens, and R. Menzel. Gravitational properties of light: The emission of counter-propagating laser pulses from atoms. *Physical Review D*, 95, 2017. URL https://journals.aps.org/prd/abstract/10.1103/PhysRevD.95.084008.

Jonathan W. Richardson, Ohkyung Kwon, H. Richard Gustafson, Craig Hogan, Brittany L. Kamai, Lee P. McCuller, Stephan S. Meyer, Chris Stoughton, Raymond E. Tomlin, and Rainer Weiss. Interferometric constraints on spacelike coherent rotational fluctuations. *Phys. Rev. Lett.*, 126:241301, Jun 2021. doi:10.1103/PhysRevLett.126.241301. URL https://link.aps.org/doi/10.1103/PhysRevLett.126.241301.

N. Rosen. Plane polarized waves in the general theory of relativity. *Phys. Z. Sowjet.*, 12: 366, 1937.

R.K. Sachs. Gravitational waves in general relativity, viii. waves in asymptotically flat spacetime. *Proc. Roy. Soc. Lond. A.*, 270, 1962. URL https://doi.org/10.1098/rspa.1962.0206.

G. Satishchandran and R. M. Wald. The asymptotic behavior of massless fields and the memory effect. *Physical Review D*, 99, 2019. URL https://journals.aps.org/prd/abstract/10.1103/PhysRevD.99.084007.

Ralf Schutzhold. Small cosmological constant from the QCD trace anomaly? *Phys. Rev. Lett.*, 89:081302, 2002. doi:10.1103/PhysRevLett.89.081302.

P C E Stamp. Rationale for a correlated worldline theory of quantum gravity. *New Journal of Physics*, 17(6):065017, jun 2015. doi:10.1088/1367-2630/17/6/065017. URL https://doi.org/10.1088/1367-2630/17/6/065017.

A.A. Starobinsky. Dynamics of phase transition in the new inflationary universe scenario and generation of perturbations. *Physics Letters B*, 117(3):175 – 178, 1982. ISSN 0370-2693. doi:https://doi.org/10.1016/0370-2693(82)90541-X. URL http://www.sciencedirect.com/science/article/pii/037026938290541X.

John D. Steele. On generalised p . p . waves. 1989. URL https://api.semanticscholar.org/CorpusID:10984869.

Andrew Strominger and Alexander Zhiboedov. Gravitational memory, BMS supertranslations, and soft theorems. 2014. URL https://arxiv.org/abs/1411.5745.

Gerard 't Hooft. The Quantum Black Hole as a Hydrogen Atom: Microstates Without Strings Attached. 2016a.

Gerard 't Hooft. Black hole unitarity and antipodal entanglement. *Found. Phys.*, 46(9): 1185–1198, 2016b. doi:10.1007/s10701-016-0014-y.

Gerard 't Hooft. Virtual black holes and space–time structure. *Foundations of Physics*, 48 (10):1134–1149, Oct 2018. ISSN 1572-9516. doi:10.1007/s10701-017-0133-0. URL https://doi.org/10.1007/s10701-017-0133-0.

M. Tanabashi et al. Review of Particle Physics. *Phys. Rev.*, D98(3):030001, 2018. doi:10.1103/PhysRevD.98.030001.

A. Tolish and R. M. Wald. Retarded fields of null particles and the memory effect. *Physical Review D*, 89, 2014. URL https://journals.aps.org/prd/abstract/10.1103/PhysRevD.89.064008.

A. Tolish, L. Bieri, D. Garfinkle, and R. Wald. Examination of a simple example of gravitational wave memory. *Physical Review D*, 90, 2019. URL https://journals.aps.org/prd/abstract/10.1103/PhysRevD.90.044060.

R. M. Wald. *General Relativity*. University of Chicago Press, 1984.

Steven Weinberg. The Cosmological Constant Problem. *Rev. Mod. Phys.*, 61:1–23, 1989. doi:10.1103/RevModPhys.61.1.

Steven Weinberg. *Cosmology*. Oxford University Press, 2008a. ISBN 9780198526827. URL http://www.oup.com/uk/catalogue/?ci=9780198526827.

Steven Weinberg. *Cosmology*. Oxford University Press, 2008b. ISBN 9780198526827. URL http://www.oup.com/uk/catalogue/?ci=9780198526827.

F. Wilczek. Quantum field theory. *Rev. Mod. Phys.*, 71:S85, 1999.

Y. B. Zel'Dovich. Cosmological Constant and Elementary Particles. *Soviet Journal of Experimental and Theoretical Physics Letters*, 6:316, November 1967.

Ya. B. Zeldovich. The cosmological constant and the theory of elementary particles. *Physics-Uspekhi*, 11(3):381–393, 1968. doi:10.1070/PU1968v011n03ABEH003927. URL http://ufn.ru/en/articles/1968/3/m/.

Kathryn M. Zurek. On Vacuum Fluctuations in Quantum Gravity and Interferometer Arm Fluctuations. 12 2020.

APPENDIX A

A.1 Tensor Harmonics

In this section we lay out some properties of tensor spherical harmonics that will be used for the mode sum in Chapter 1. Consider a tensor field with spin s. We can decompose any tensor on the sphere into a mode sum over rank s tensors weighted by spherical harmonics $Y_{l,m}$ in the following manner

$$\mathcal{Y}_{j,l,s,m} = \sum_{m_l=-l}^{l} \sum_{m_s=-s}^{s} \langle l, m_l; s, m_s | j, m \rangle Y_{l,m_l} t_{s,m_s} \tag{A.1}$$

$$= \sum_{m_s=-s}^{s} \langle l, m - m_s; s, m_s | j, m \rangle Y_{l,m-m_s} t_{s,m_s} \tag{A.2}$$

where the t_{s,m_s} are a basis of spin s unit tensors satisfying

$$t^*_\alpha \cdot t_\beta = \delta_{\alpha,\beta} \tag{A.3}$$

and the $\langle \_ | \_ \rangle$ are Clebsch-Gordon coefficients. For the case of gravitational radiation, we will be concerned with $s = 2$ tensor harmonics, specifically the transverse ones, which can be separated into "electric" (E) and "magnetic" (M) parts. Here, the dot product between spin 2 tensors is taken to mean

$$A \cdot B = \sum_{i,j} A_{i,j} B_{i,j} \tag{A.4}$$

To extract the angular spectrum of a rank two tensor defined on the sphere, we can use rank 2 tensor spherical harmonics. Define the rank 2 tensor spherical harmonics

$$(T_{j,\ell,m})_{ab}(\Omega) = \mathcal{Y}_{j,\ell,2,m}(\Omega) = \sum_{\alpha,\beta} \langle \ell, \alpha; 2, \beta | j, m \rangle Y_{\ell\alpha}(\Omega) (t_\beta)_{ab} \tag{A.5}$$

where the t_α are a set of orthonormal rank 2 tensors. These tensor harmonics satisfy an orthogonality relation given by

$$\int d\Omega (T^*_{j',\ell',m'})_{ab} (T_{j,\ell,m})^{ab} = \delta_{j,j'} \delta_{\ell,\ell'} \delta_{m,m'} \tag{A.6}$$

The choice of basis employed here for the t_α is

$$t_2 = \frac{1}{2}(\hat{x}\hat{x} - \hat{y}\hat{y}) + \frac{i}{2}(\hat{x}\hat{y} + \hat{y}\hat{x}) \tag{A.7}$$

$$t_1 = -\frac{1}{2}(\hat{x}\hat{z} + \hat{z}\hat{x}) - \frac{i}{2}(\hat{y}\hat{z} + \hat{z}\hat{y}) \tag{A.8}$$

$$t_0 = \frac{1}{\sqrt{6}}(2\hat{z}\hat{z} - \hat{x}\hat{x} - \hat{y}\hat{y}) \tag{A.9}$$

$$t_{-1} = \frac{1}{2}(\hat{x}\hat{z} + \hat{z}\hat{x}) - \frac{i}{2}(\hat{y}\hat{z} + \hat{z}\hat{y}) \tag{A.10}$$

$$t_{-2} = \frac{1}{2}(\hat{x}\hat{x} - \hat{y}\hat{y}) - \frac{i}{2}(\hat{x}\hat{y} + \hat{y}\hat{x}) \tag{A.11}$$

$$(t^*_\alpha)^{ab} (t_\beta)_{ab} = \delta_{\alpha\beta} \tag{A.12}$$

Any tensor function defined on the sphere can be decomposed into a series of these tensor harmonics.

$$f_{ab}(\Omega) = \sum_{j,\ell,m} C_{j,\ell,m} (T_{j,\ell,m})_{ab}(\Omega) \tag{A.13}$$

The coefficients can be extracted using the orthogonality properties of the tensor harmonics.

$$C_{j,\ell,m} = \int d\Omega (T^*_{j,\ell,m})^{ab} f_{ab} \tag{A.14}$$

Finally, we recall the definition of the Spherical Harmonics, Legendre Polynomials, and Associated Legendre Polynomials.

$$Y_{\ell m}(\theta,\phi) = \sqrt{\frac{2\ell+1}{4\pi}} \sqrt{\frac{(\ell-m)!}{(\ell+m)!}} P^m_\ell(\cos\theta) e^{im\phi} \tag{A.15}$$

$$P_\ell^m(x) = (-1)^m(1-x^2)^{m/2}\frac{d^m}{dx^m}P_\ell(x) \quad (m \geq 0) \tag{A.16}$$

$$P_\ell^{-m} = (-1)^m\frac{(\ell-m)!}{(\ell+m)!}P_\ell^m \tag{A.17}$$

$$P_\ell(x) = \frac{1}{2^\ell \ell!}\frac{d^\ell}{dx^\ell}(x^2-1)^\ell \tag{A.18}$$

A.1.1 Transverse Tensor Spherical Harmonics

As mentioned above, there are two types of transverse tensor harmonics.

$$T^E_{l,m} = \sqrt{\frac{(l+1)(l+2)}{2(2l+1)(2l-1)}}T_{l,l-2,m} + \sqrt{\frac{3(l-1)(l+2)}{(2l-1)(2l+3)}}T_{l,l,m} + \sqrt{\frac{l(l-1)}{2(2l+1)(2l+3)}}T_{l,l+2,m} \tag{A.19}$$

$$T^M_{lm} = \sqrt{\frac{l+2}{2l+1}}T_{l,l-1,m} + \sqrt{\frac{l-1}{2l+1}}T_{l,l+1,m} \tag{A.20}$$

These satisfy orthogonality conditions given by

$$\int d\Omega T^E_{lm}\cdot T^{E*}_{l'm'} = \delta_{ll'}\delta_{mm'} \tag{A.21}$$

$$\int d\Omega T^M_{lm}\cdot T^{M*}_{l'm'} = \delta_{ll'}\delta_{mm'} \tag{A.22}$$

One can show using a series of recursion relations that the transverse harmonics have the following explicit form

$$T^E_{l,m} = (\hat{\theta}\hat{\theta} - \hat{\phi}\hat{\phi})\frac{1}{\sqrt{2l(l+1)(l-1)(l+2)}}\left(2\frac{\partial^2}{\partial\theta^2} + l(l+1)\right)Y_{l,m} \tag{A.23}$$
$$+ (\hat{\theta}\hat{\phi} + \hat{\phi}\hat{\theta})\sqrt{\frac{2}{l(l+1)(l-1)(l+2)}}im\frac{\partial}{\partial\theta}\left(\frac{Y_{l,m}}{\sin\theta}\right)$$
$$T^M_{lm} = -(\hat{\theta}\hat{\theta} - \hat{\phi}\hat{\phi})\sqrt{\frac{2}{l(l+1)(l-1)(l+2)}}m\frac{\partial}{\partial\theta}\left(\frac{Y_{l,m}}{\sin\theta}\right) \tag{A.24}$$
$$- (\hat{\theta}\hat{\phi} + \hat{\phi}\hat{\theta})\frac{1}{\sqrt{2l(l+1)(l-1)(l+2)}}\left(2\frac{\partial^2}{\partial\theta^2} + l(l+1)\right)Y_{l,m}$$

A.1.2 Memory Decomposition

First, we apply these definitions to the memory tensor defined in Chapter 1, Section . We take the result from eq. (1.13) and expand in a basis of transverse tensor harmonics. Note importantly that the transverse tensor harmonics are not defined for $l < 2$. In the case we are considering, we have axisymmetry, so only the $m = 0$ modes contribute. Looking at the form of eq. (1.13), we see that we must have that

$$\Delta D = \frac{M}{r}\left(\sum_{l=2}^{\infty} a_l T^E_{l,0}\right)\cdot D_0 \tag{A.25}$$

We can determine the a_l using the orthogonality condition eq. (60).

$$
\begin{aligned}
a_l &= \int d\Omega T^{E*}_{l,0} \cdot (\hat{\theta}\hat{\theta} - \hat{\phi}\hat{\phi}) \\
&= \sqrt{\frac{2}{l(l+1)(l-1)(l+2)}} \sqrt{\frac{2l+1}{4\pi}} \int d\Omega \left(2\frac{d^2}{d\theta^2} + l(l+1) \right) P_l(\cos\theta) \\
&= -\sqrt{\frac{2\pi(2l+1)}{l(l+1)(l-1)(l+2)}} \int d\cos\theta \left(2\cot\theta \frac{d}{d\theta} + l(l+1) \right) P_l(\cos\theta) \\
&= 2\sqrt{\frac{2\pi(2l+1)}{l(l+1)(l-1)(l+2)}} \int dx x \frac{d}{dx} P_l(x) \\
&= 4\sqrt{\frac{2\pi(2l+1)}{l(l+1)(l-1)(l+2)}} \quad (l \text{ even})
\end{aligned}
\tag{A.26}
$$

APPENDIX B

B.1 Curvature Identities

Here we summarize some curvature identities that are referenced in the work. The first is the Bianchi identity

$$\nabla_{[a}R_{bc]de} = 0 \tag{B.1}$$

The first contracted Bianchi identity is

$$\nabla^a R_{abcd} = \nabla_c R_{db} - \nabla_d R_{cb} \tag{B.2}$$

Taking the divergence of the Bianchi identity gives

$$\Box R_{bcde} = -\nabla^a \nabla_b R_{cade} - \nabla^a \nabla_c R_{abde} \tag{B.3}$$

The Riemann curvature tensor can be decomposed into its totally trace-free part (Weyl tensor) and it's trace (Ricci tensor and scalar).

$$R_{abcd} = C_{abcd} + \frac{1}{2}(R_{ac}g_{bd} - R_{ad}g_{bc} - R_{bc}g_{ad} + R_{bd}g_{ac}) + \frac{R}{6}(g_{ad}g_{bc} - g_{ac}g_{bd}) \tag{B.4}$$

In general, the antisymmetric covariant derivative on any tensor can be related to the Riemann curvature tensor via

$$(\nabla_a \nabla_b - \nabla_b \nabla_a) T^{c_1 \ldots c_m}_{d_1 \ldots d_n} = -\sum_i R_{abe}{}^{c_i} T^{c_1 \ldots e \ldots c_m}_{d_1 \ldots d_n} + \sum_j R_{abd_j}{}^{e} T^{c_1 \ldots c_m}_{d_1 \ldots e \ldots d_n} \tag{B.5}$$

It then follows that in the linearized theory, we have

$$(\nabla_a \nabla_b - \nabla_b \nabla_a) R_{cdef} = 0 \tag{B.6}$$

Using eq. B.6, B.4 and the Einstein field equations in eq. B.3 we have a linearized wave equation for the Riemann tensor.

$$\Box R_{abcd} = -32\pi\nabla_{[a}\nabla_{|[d}T_{c]|b]} - 16\pi\eta_{[c[b}\nabla_{a]}\nabla_{d]}T \tag{B.7}$$

B.2 Timelike Congruences

Consider a congruence of timelike geodesics whose tangent vectors are defined by the vector field $u^a(x^\mu)$. We can define the expansion θ, shear σ_{ab}, and twist ω_{ab} of the congruence by examining the tensor field $\nabla_a u_b$. Define the metric q_{ab} of the 3 dimensional hypersurface orthogonal to u^a via the relation $g_{ab} = -u_a u_b + q_{ab}$. Then we have

$$\theta = q^{ab}\nabla_a u_b \tag{B.8}$$

$$\sigma_{ab} = \nabla_{(a}u_{b)} - \frac{1}{3}\theta q_{ab} \tag{B.9}$$

$$\omega_{ab} = \nabla_{[a}u_{b]} \tag{B.10}$$

The geodesic deviation equation then gives an evolution equation for the expansion, shear, and twist.

$$\frac{d}{d\tau}\theta = -R_{ab}u^a u^b + 2\omega^2 - 2\sigma^2 - \frac{1}{3}\theta^2 \tag{B.11}$$

$$\frac{d}{d\tau}\sigma_{ab} = C_{cbad}u^c u^d + \frac{1}{2}\tilde{R}_{ab} - \frac{2}{3}\theta\sigma_{ab} - \sigma_{ac}\sigma^c{}_b - \omega_{ac}\omega^c{}_b + \frac{1}{3}q_{ab}(\sigma^2 - \omega^2) \tag{B.12}$$

$$\frac{d}{d\tau}\omega_{ab} = -\frac{2}{3}\theta\omega_{ab} - 2\omega_{c[a}\sigma_{b]}{}^c \tag{B.13}$$

where

$$\tilde{R}_{ab} = q_{ac}q_{bd}R^{cd} - \frac{1}{3}q_{ab}q_{cd}R^{cd} \tag{B.14}$$

In the linearized and low velocity regime, these equations reduce to

$$\frac{d}{dt}\theta \approx -R_{00} \tag{B.15}$$

$$\frac{d}{dt}\sigma_{ab} \approx C_{0ba0} + \frac{1}{2}\tilde{R}_{ab} \tag{B.16}$$

$$\frac{d}{d\tau}\omega_{ab} \approx 0 \tag{B.17}$$